The Pennsylvania State University

The Graduate School

SYNTHESIS AND CHARACTERIZATION OF CITRATE-BASED BIODEGRADABLE MATERIALS AND THEIR APPLICATIONS

A Dissertation in

Bioengineering

by

Qiyao Li

Submitted in Partial Fulfillment

of the Requirements

for the Degree of

Doctor of Philosophy

August 2020

The dissertation of Qiyao Li was reviewed and approved by the following:

Jian Yang

Professor of Biomedical Engineering and Dorothy Foehr Huck and J. Lloyd Huck Chair in Regenerative Engineering

Dissertation Advisor

Chair of Committee

Qing Wang

Professor of Materials Science and Engineering

Nanyin Zhang

Professor of Biomedical Engineering and Dorothy Foehr Huck and J. Lloyd Huck Chair in Brain Imaging

Pak Kin Wong

Professor of Biomedical Engineering and Mechanical Engineering

Daniel Hayes

Professor of Biomedical Engineering

Dorothy Foehr Huck and J. Lloyd Huck Chair in Nanotherapeutics and Regenerative Medicine

ABSTRACT

Bioactive polymeric materials with the capability of regulating cell differentiation, adhesion, and migration hold great potential for many tissue engineering applications, such as bone and nerve regeneration, drug delivery, and so on. Additionally, polymeric materials gained popularity in agriculture, food, and construction industry due to their easily tunable mechanical and degradation properties achieved by manipulating polymerization conditions, composites formulation, and processing techniques. As needs across the engineering field have evolved and require increasingly sophisticated solutions, citrate-based biomaterials provide unique physical, chemical, and biological properties that can be customized to meet the complicated and specific requirements of regenerative engineering and other biomedical applications.

We researched and investigated the citrate-based polymeric materials' degradation behavior and mechanism, development of a new class of osteopromotive citrate-based materials with glycerophosphate salts for bone tissue engineering applications, and utilization of citrate-based resin in vegetable oil filtration. This scientific work aims to develop a variety of versatile citrate-based polymers and explore and demonstrate their applications in biomedical and vegetable oil purification fields.

TABLE OF CONTENTS

LIST OF FIGURES

LIST OF TABLES

ACKNOWLEDGMENTS

I would like to thank Dr. Jian Yang and my colleagues at the transformative biomaterials' lab for their tremendous support throughout my Ph.D. program. I would also like to thank my parents and my boyfriend for their support and for teaching me the high value of work ethics and dedication, without which I would not have been able to complete my doctoral degree. Additionally, I would like to thank my friends at Penn State for being a constant source of encouragement throughout the entire five years of my Ph.D. experience.

This material is based upon work supported by the NSF under Award No CMMI 1537008, NIH under No.AR072731, Ohio Soybean Council research grant under No.18-R-31.

Any opinions, findings, and conclusions or recommendations expressed in this publication are those of the author(s) and do not necessarily reflect the views of the NSF, NIH, and Ohio Soybean Council.

1 Chapter

INTRODUCTION

1.1 Bone regeneration

As a dynamic organ, bone is continuously remodeling to self-repair damages arising due to fatigue, wear, and tear. A bone matrix is made of four groups of cells: osteoblasts, osteocytes, osteoclasts, and bone lining cells. These cells assist in building and maintaining this matrix and remodel it when needed. Osteoblasts are in charge of producing the bone matrix while mature osteoblasts, also referred to as osteocytes, whose function is to maintain the bone matrix, and osteoclasts are in charge of degrading and eradicating the matrix of old and/or damaged tissue. Meanwhile, osteoblasts are responsible for resulting osteogenic differentiation of mesenchymal stem cells (MSCs) [1], when damage occurs that is beyond the self-repairing capabilities of natural bone [2-3]. With over 2 million bone grafting procedures conducted each year around the world and an increasingly aging global population, it demands for improved bone grafting procedures and regenerative technologies [4-5].

Nowadays, autografts gain popularity as a standard procedure for bone grafting, which involves tissue harvest from the patient. While the autograft has been an effective procedure, there are numerous limitations that demand for further improvements. First of all, additional surgery for the patient is needed in autografts, which could result in further

implications such as infection or donor site morbidity that refers to both short-term and occasional long-term pain, which is experienced by approximately 20% of autograft patients. Secondly, only a limited supply of tissue can also be harvested, which is a problem in the clinic. While allografts surpass the limitations of donor-site morbidity and supply, the risk of disease transmission and alteration of mechanical and biological properties from sterilization is of concern. Both autograft and allograft procedures possess benefits, but their inherent concerns call for the need for alternatives.

1.2 Biomaterials for orthopedic engineering

A variety of grafts are used for bone regeneration: autograft, allograft, naturally occurring materials, polymeric materials, metals, and ceramics. Synthetic polymers gained their popularity due to defined chemistry, versatile functionality, great processability, and tunability. A new generation of synthetic biomaterials for bone grafting is expected to have biodegradable and tissue-specific physicochemical features to guide cell behavior and tissue morphogenesis. To overcome the shortcomings of being bioinert and elicit an undesirable inflammatory response, biomolecules have been applied to endow synthetic polymers' specific characteristic manner. However, uncontrollable release, inefficient loading, and intricate chemistry are the challenges researchers face when engineering polymer scaffolds with bioactive molecules. Moreover, most modifications to polymer scaffolds can either functionally improve bioactivities or only structurally grant them better mechanical properties. Therefore, an easily accessible and efficient way to achieve both goals is desired.

Hydrogels, another type of polymeric scaffolds, are widely used for bone regeneration. Among hydrogels, injectable hydrogels are more favorable, allowing encapsulated cells and/or drugs to be delivered via syringe to target sites with precise control through a small incision. Injectable hydrogels fall into two main categories based on their crosslinking mechanism: physically and chemically crosslinked hydrogels. For physical crosslinking, the sol-gel transition occurs under the effects of pH [1], enzymes [2-3], temperature [4-5], crosslinkers [6] or ionic strength [7] caused by the environmental differences between *ex vivo* and *in vivo* conditions. Physical crosslinking includes ionic/electrostatic interaction, crystallization, hydrogen bonding, and ultrasonication mediated sol-gel transition [8-9]. Chemical crosslinking, a process of binding polymer chains together by covalent bonds, usually involves photo-polymerization, Michael addition polymerization, radical polymerization, or redox-initiated reactions [10]. However, both chemical and physical crosslinking have their shortcomings. Formation of a physically crosslinked hydrogel is usually milder and more cell-friendly but usually results in poor mechanical properties that may not satisfy the requirements of complicated applications in which toughness and strength are required. On the other hand, chemical crosslinking mechanisms have more potential to trigger inflammation due to cytotoxic crosslinkers, burst release of byproducts (i.e., initiators) in the microenvironment, or necrosis from UV light exposure [11]. Thus, novel classes of catalyst-free, non-cytotoxic, and injectable hydrogels are required to allow better tissue ingrowth.

1.3 Citric acid

Most commonly known as an intermediate product of the Krebs cycle, citric acid has several functions, plays a critical role in metabolic and mineral regulation, and also possesses antimicrobial, anticoagulant, and osteopromotive properties (**Figure** 0.1). As an indispensable component in bone, citrate makes up for about 5 wt % of the total organic content in bone and plays a significant role in intrinsically regulating bone hydroxyapatite-like (HA) minerals and biologically affecting cell's metabolism [12-14]. Additionally, solute citrate is proven to promote endothelial sprouting in rat aortic rings and increase the production of angiogenic growth factors [15]. The new blood vessel formation is also necessary for transporting growth factors and nutrients during bone formation.

Citric acid, the main functional monomer of citrate-based biomaterials, also happens to be found in significant quantities within bone tissue, proven to be vital for the stability, strength, and fracture resistance of bone tissue. Since citric acid has pKa values of 2.9, 4.3, and 5.6, citric acid mostly present in the form of citrate in most human tissues.

Bone is a dynamic organ, able to replace old or disrupted bone tissue through a remodeling process. The bone tissue has a matrix-like structure, which is comprised of collagen. Collagen, the major supportive tissue of the body, is responsible for protecting vital organs and provide calcium and phosphate storage. Citrate in human body plays a vital role in the maintenance of energy homeostasis in cells and over 90% is stored in the bone tissue matrix [16]. Carboxylate groups are confirmed to be crucial to the regulation of the formation of apatite in bone and that aside from collagen, while citrate provides more carboxylate functional groups than any other molecule in bone combined. Additionally,

citrate is a better stabilizer of hydroxyapatite crystals than other phosphates, crucial for the maintenance of bone stability, strength, and resistance to fracture [17-18]; however, citrate's effect on local molecular composition and surface structures has largely not yet understood [19].

1.4 Citrate-based polymers

As a non-toxic, readily available and cost-efficient molecule, citric acid is used as the backbone monomer or crosslinker to develop a group of poly(diol citrates). These citrate-based polymers comprise widely tunable mechanical properties and degradation rates and release profile. Also, they possess various antioxidant, antimicrobial, adhesive and fluorescent properties, unique in biomedical applications.

First of all, the chemically active nature of citric acid, comprised of three carboxyl groups and one hydroxyl group, presenting crucial functionality for citrate-based biomaterials [12]. Mostly, the carboxyl groups react with hydroxyl groups from diols to form ester groups and then polyesters. After polycondensation, some carboxyl and hydroxyl groups are partially preserved, enabling inherent functionality, surface modification, chelation or crosslinking. These functional structure enables the development of the unique properties of citrate-based biomaterials as versatile tools for both *in vitro* and *in vivo* biomedical applications [16] and even food science fields.

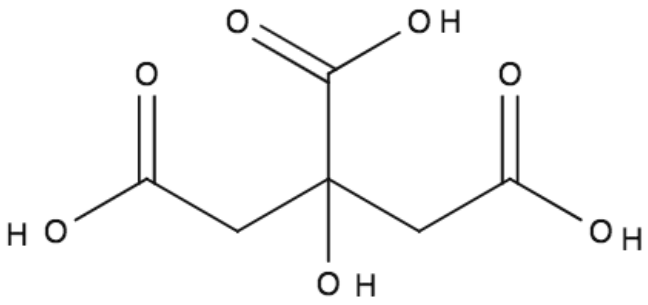

Figure 0.1 Chemical structure of citric acid.

β-glycerophosphate disodium (βGP-Na), as an organic sodium salt, is widely utilized as a supplement in osteogenic media [20]. Glycerophosphate calcium (GP-Ca) is commonly used as a dietary supplement. In general, glycerophosphates possess a potential for mineralization, adhesion, and proliferation [21]. Previously, based on the osteopromotive potential of these salts, the two types of salts were incorporated into POC via the functional opportunities of citric acid to yield POC-GP. The addition of GP salts enhances the bioactivity of the material and to enhance the osteogenic differentiation of human mesenchymal stem cells (hMSCs). Besides, addition of GP enhanced mechanical properties, and adjustment of ion type, crosslinking conditions and feeding ratio of GP to citric acid allows for convenient tuning of mechanical properties, degradation, release profile, and osteopromotive activities.

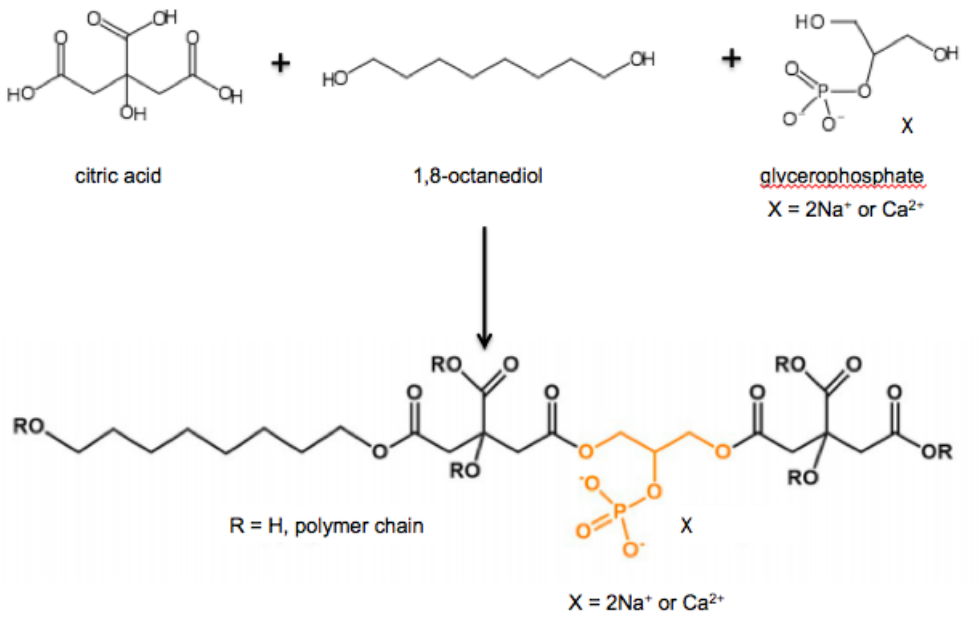

Figure 0.2 Incorporation of glycerophosphate salts into the poly(octamethylene citrate) polymer chain.

1.5 Glycerophosphate

β-glycerophosphate disodium (βGPNa), widely known as an osteogenic medium supplement and a weak base, has been used to initiate the gelation of chitosan or collagen to generate thermosensitive injectable hydrogels [20]. Another GP salt, glycerophosphate calcium (GPCa), representing as a mixture of β-isomer (80%) and rac-α-isomer (20%), has long been used as a food supplement for both calcium and phosphate. Given the osteopromotive benefits of these salts in their solute and conjugated form [21-23], we incorporated two types of GP salts into the citrate-based materials through a one-pot polycondensation reaction by taking advantage of the reactive nature of citric acid, as shown in **Figure** 0.2, to prepare POC-GP and further improve the bioactivity of citrate

materials to promote stem cell osteogenic differentiation. POC-GP/HA composite disks and microparticles were evaluated for their ability to enhance osteogenic differentiation of hMSCs. In tissue regeneration, biomaterial scaffolds are a crucial piece of the puzzle, acting as a guide for tissue growth. Composite scaffolds, composed of a synthetic polymer and an inorganic filler, possess high mechanical strength and bioactivity, combining the advantages of both materials. One major challenge of scaffolds for bone tissue engineering is the compromise between scaffold strength and porosity. Strong mechanical properties are necessary for the scaffold to be compatible with the existing bone; however, the scaffold must be porous enough to allow for good cell penetration, vascularization, and diffusion of nutrients and waste products. The use of microparticles allows for more natural cell to cell interactions and cell to particle contacts [24-25], and eliminates the need for cells to infiltrate the pores of a biomaterial, as is necessary for the use of traditional bulk scaffolds [24, 26-27]. Additionally, incorporation of microparticles in cell cultures improves oxygen delivery, nutrient, and waste diffusion through the prevention of gap junction formation [27-28]. The surface roughness of microparticles and their size has been shown to play a role in stem cell behavior.

1.6 Polymer degradation and erosion

The utilization and effectiveness of any materials depend on their degradability, immovability, and durability. According to the American Society for Testing of Materials (ASTM), degradable plastics are defined as polymers that change their chemical structure in certain environmental conditions resulting in a significant alteration in physical and mechanical properties. To be more specific, polymer degradation can be divided into

abiotic and biotic processes [29]. In the abiotic process, the degradation profile can be majorly attributed to the formation of polymer or oligomer radicals caused by some external driving force, including temperature, mechanical stress, solvent, radiation, pH, etc. [30]. The development of unstable radicals during the formation of stable polymers with oxygenated groups results in distinct changes in molecular weight, PDI, branching, end functional groups, etc., and even the formation of crosslinked structures. The reactions between small molecules, macromolecules, small radicals, and macroradicals may give rise to many competitive reactions and more complicated degradation paths, leading to strongly different final properties of polymers. For instance, the combination between macromolecules and macroradicals can give rise to improved molecular weight and the polymer properties, while the reactions between small molecules or small radicals with macromolecules can give rise to the faster breaking of the polymer chains [31].

The interplay between the physical properties of polymer chains and their dimensions is one of the main goals of polymer science. After the decades of the dedication of researchers' contribution, it allowed us to determine the correlation between chain dimensions, density, glass transition temperature, plateau modulus, etc., carried out with computational models [32]. Thus, the comprehensive understanding of polymer chain structures after degradation can give rise to an accurate prediction of pure polymers, polymer blends, and polymer composites properties based on the structure-property associations. The polymer composites' degradation behavior can be significantly affected by the degradation routes of the pure polymer and inorganic fillers. The interactions among different species and degradation products can also occur during degradation [30]. Polymer blends also present different degradation behaviors because a stable pure polymer may

progress to be less stable when blended with another pure polymer since the second polymer phase can extract a hydrogen atom from the first polymer phase, resulting in macroradicals.

Biotic degradation, also referred to as biodegradation, is widely used in polymers for the local drug delivery, target cancer and against organ failure treatment, development of vaccines, and orthopedic fixing devices. Degradable materials are classified as materials that degrade during or immediately after their application and "non-degradable" are polymers that require a significantly longer time to degrade than the duration of their application. Therefore, the definitions for degradation and erosion vary distinctly based upon applications [33]. In most cases, degradation refers to the process of chain scission during which polymer chains are cleaved to form oligomers or monomers, while erosion describes the loss of material because of oligomers and monomers leaving the polymer [31]. During polymer erosion, water enters the polymer bulk, resulting in swelling of polymer and chemical degradation, which is accompanied by the creation of oligomers and monomers [33]. The degradable polymer erosion is classified by the surface (heterogeneous) erosion and bulk (homogeneous) erosion. **Figure** 0.3 illustrates the peculiarity between the surface and bulk erosion [34]. Surface erosion describes the process of polymers by which they lose material from the surface only and get smaller is size while keeping their original geometric shape. The bulk erosion of polymers is not restricted to the surface; thus, the size of polymer bulk will remain the same for a considerable length of time during its application [35].

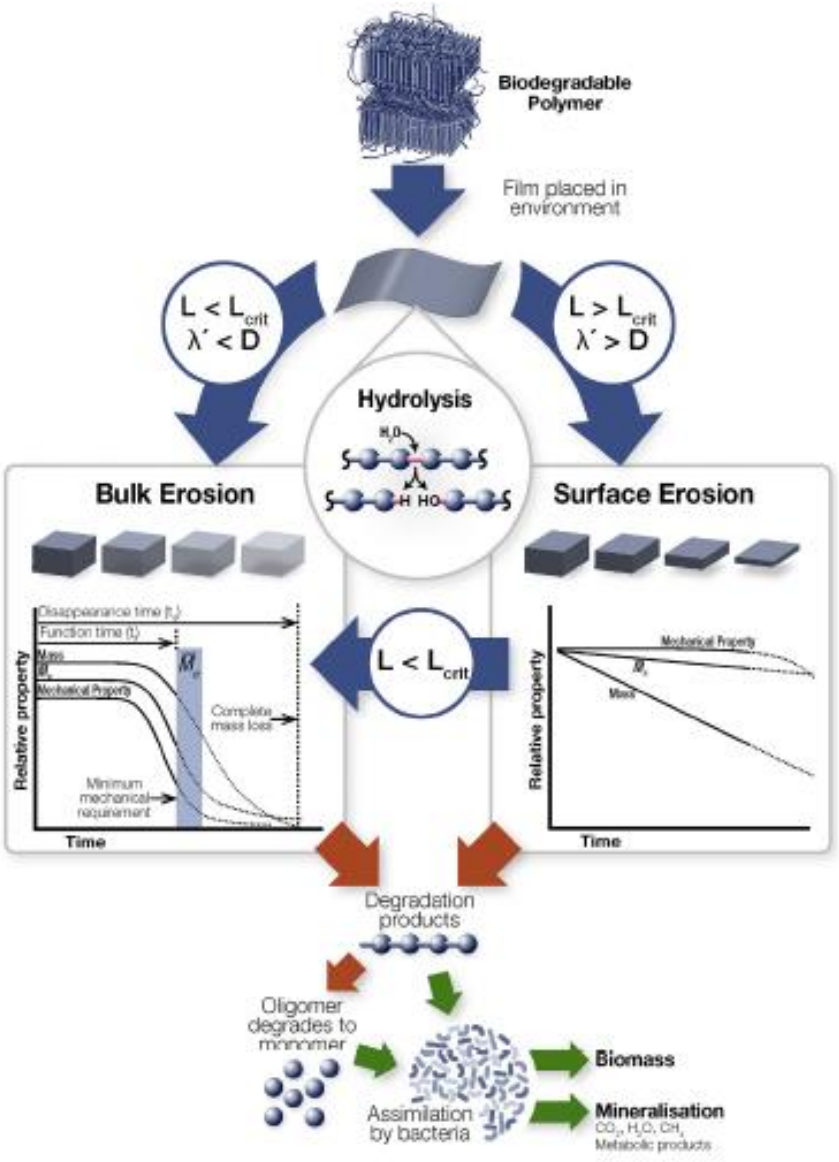

Figure 0.3 A schematic illustrates the general hydrolytic degradation and erosion processes in these polymers [34].

1.7 Molecular weight determination

The polymer molecular weight can be defined and characterized in different ways based on various theories. The combination of size exclusion chromatography and MALS (SEC-MALS) is used to measure the absolute molar mass and size distributions of macromolecules in solution. The concentration sensitive detector is a differential refractometer (dRI). Since the existence of SEC-MALS, the weight-averaged molecular weight can be determined independently of retention time and molecular standards which overcomes the limitations of column calibration. Weight-average molar mass was measured by MALS directly while the number-average molar mass was calculated based on the MALS and dRI.

M_n was calculated by Equation 1:

$$\bar{M}_n = \frac{\Sigma n_i M_i}{\Sigma n_i} = \frac{\Sigma c_i}{\Sigma\, c_i / M_i} \qquad \textbf{Equation 1.1}$$

M_w was calculated by Equation 2:

$$\bar{M}_w = \frac{\Sigma n_i {M_i}^2}{\Sigma n_i M_i} = \frac{\Sigma c_i M_i}{\Sigma c_i} \qquad \textbf{Equation 1.2}$$

The Polydispersity index (PDI) was calculated by Equation 1.3:

$$PDI = \bar{M}_w / \bar{M}_n \qquad \textbf{Equation 1.3}$$

Here n_i is the number of molecules with molecular weight of M_i; c_i is the weight concentration of molecules with molecular weight of M_i, which is measured by the refractive index detector; M_i is the molecular weight for each slice in the chromatogram which is calculated from the intensity of the scattered light.

2 Chapter

SYNTHESES AND PHYSICAL AND CHEMICAL CHARACTERIZATION OF CITRATE-BASED POLYMERS AND COMPOSITES

2.1 Introduction

In recent years, citrate-based polymeric biomaterials have gained significant attention in tissue engineering, drug delivery, food processing and many other related applications. However, the degradation behavior and mechanism of citrate-based polymers have not been clearly and systematically investigated, lacking a comprehensive guidance and reference in terms of citrate-based polymers' degradation and erosion properties in various applications [36].

Building on the recent development of citrate-based polymers and their various applications, here we further developed a series of citrate-based polymers by using different monomers to react with citric acid through one-pot bulk polymerization, such as xylitol, glycerophosphate disodium and glycerophosphate calcium and in accordance with the previous studies, we used monomers such as octanediol and hexamethylene,. The resulting polymers, for example, poly(octamethylene citrate) (POC), poly(hexamethylene citrate) (PHC), poly(octamethylene citrate xylitol) (POCX), poly(octamethylene citrate glycerophosphate sodium) (POC-βGP-Na), poly(octamethylene citrate glycerophosphate calcium) (POC-GP-Ca), were studied as the representative citrate-based polymers to investigate the polymer degradation behavior.

Specifically, 1, 6-hexanediol was used to replace 1,8-octanediol in POC to investigate the synthesis and degradation performance differences between polymers with a shorter diol chain length.

Besides, β-glycerophosphate disodium (βGPNa) and glycerophosphate calcium (GPCa), known as an osteogenic medium supplement and a food supplement for both calcium and phosphate, respectively. Given the osteopromotive benefits of these salts in their solute and conjugated form [21-23], we incorporated two types of GP salts into the citrate-based materials by taking advantage of the reactive nature of citric acid and investigated the degradation properties.

Xylitol, as a naturally occurring sugar which can be widely found in common fruits, vegetables and plants, is used as a food additive and sugar substitute. Recently, more and more researchers used xylitol as a structural block in polymerization in biomedical engineering field, which possesses a wide range of physical properties that are biologically relevant. For example, xylitol-based degradable hydrogel or elastomers showing a great biocompatibility *in vitro* and *in vivo* and a promotion in bone density and bone mineral content since it assists in a better calcium absorption in the same way as a vitamin D does [37]. Besides, due to the excellent water solubility, xylitol was used to tune polymer's degradation profiles effectively, herein for citrate-based polymers. In this study, the POC doped with xylitol demonstrated an extraordinarily rapid degradation rate compared to POC and other citrate-based polymers, suggesting xylitol could serve as an effective tool to tune citrate polymer degradation.

2.2 Materials and methods

2.2.1 Materials

HA [(particle size: >75 μm (0.5%), 45–75 μm (1.4%), <45 μm (98.1%)] was purchased from Fluka (St Louis, MO). 1,8-octanediol (98%), 1,6-hexanediol, and citric acid (99.5%) were purchased from Alfa Aesar. B-glycerophosphate-Na (βGPNa), Glycerophosphate-Ca (GPCa), xylitol, and all remaining chemicals were purchased from Sigma-Aldrich (St Louis, MO) and used as received unless stated otherwise. Dimethylformamide (DMF, Sigma-Aldrich, HPLC grade, Catalog # 648531).

2.2.2 Pre-polymer synthesis

POC pre-polymer was synthesized by bulk polymerization using citric acid and 1,8-octanediol in 1.0:1.1 feeding ratio. Briefly, monomers were stirred mechanically and melted under nitrogen protection at 160°C in a silicon oil bath. Then the temperature of the system was lowered to 140°C, followed by stirring for 1-2 hours to create the pre-polymer. Then the reaction was quenched by 1,4-dioxane and purified in deionized water followed by lyophilization. The purified pre-polymer was dissolved in 1,4-dioxane (30 wt/wt%) for future uses. PHC, POC-βGP-Na, POC-GP-Ca, and POCX pre-polymers were all synthesized in the same method as mentioned above with citric acid, 1,8-octanediol, 1, 6-hexanediol, β-glycerophosphate disodium (β-GPNa), glycerophosphate calcium (GPCa)

and xylitol (X) in different feeding ratios as shown in Table 1, except that dialysis was performed to purify the pre-polymer before freeze drying.

Table 1 Formulations of pre-polymer synthesis

	Citric acid (M)	**Diol (M)**	**Additonal monomer**
POC	1.0	1.1 (1,8-Oactandiol)	/
PHC	1.0	1.1 (Hexanediol)	/
POCX	1.0	0.5 (1,8-Oactandiol)	0.6 (Xylitol)
POC-(0.2)βGP-Na	1.0	0.9 (1,8-Oactandiol)	0.2 GP-Na
POC-0.3βGP-Na	1.0	0.8 (1,8-Oactandiol)	0.3 GP-Na
POC-0.5βGP-Na	1.0	0.6 (1,8-Oactandiol)	0.5 GP-Na
POC-0.2GP-Ca	1.0	0.9 (1,8-Oactandiol)	0.2 GP-Ca
POC-(0.3)GP-Ca	1.0	0.8 (1,8-Oactandiol)	0.3 GP-Ca

2.2.3 Preparation of polymer films, polymer/HA composites

To prepare polymer films, pre-polymer solution was casted in Teflon dishes and the solvent was allowed to evaporate. The dried pre-polymer was then thermally crosslinked at 80°C for 3 days and then at 120°C with vacuum for 1 day to obtain a crosslinked polymer film. To prepare polymer/HA composites, a 30% pre-polymer solution in 1,4-dioxane solvent was mixed with hydroxyapatite (HA) by continuously stirring. The pre-polymer solid content to HA ratio is 60:40 by weight. After the mixture turned dough-like, it was then pressed into thin sheets. The composite sheets were cut into round disks before thermally crosslinked at 80°C for 3 days and then at 120°C with vacuum for 1 day.

2.2.4 Structural characterizations

To check the chemical structural difference between POC, POC-βGP-Na and POC-GP-Ca, Fourier transform infrared (FT-IR) analysis was operated by casting polymer solution in 1,4-dioxane on KBr pellet using Bruker Vertex V70 spectrometer. FT-IR spectra were recorded over a wavelength range of 400-4000 cm^{-1}. ^{31}P NMR (161.9 MHz) spectra of pre-polymer solutions were obtained using Bruker DPX 400 NMR Spectroscopy. Either D_2O or DMSO were used as solvents. All chemical shifts were reported in ppm (δ).

2.2.5 Contact angle measurements

The water-in-air contact angles on crosslinked polymer films were measured at room temperature within 10 s after water was dropped on the film surface by a Rame-Hart goniometer and imaging system (Rame-Hart Inc., Mouttain Lake, NJ) using the sessile

drop method. Four independent measurements at different sites were averaged. The change of water-in-air contact angle with time was monitored over 60s after water dropping.

2.2.6 Mass loss study

Degradation properties were studied *in vitro* with polymer film samples placed in tubes containing 10 mL of NaOH solution (0.05 M) or phosphate buffered saline (PBS, pH=7.4) and incubated at 37°C. Samples were weighed before degradation to find the initial mass (W_0). At each determined time point, samples were washed thoroughly with deionized water 3 times. After lyophilization, samples were weighed to measure the remaining mass (W_t). Six parallel specimens were averaged for each sample, and the results were presented as means ± standard deviation. The percent mass loss was calculated based on the following equation:

$$Mass\ loss\ (\%) = \frac{W_0 - W_t}{W_0} \times 100 \qquad Equation\ (2.1)$$

2.2.7 Calcium and phosphorus release

Accumulative phosphorus and calcium release content were investigated by inductively-coupled plasma emission spectroscopy (ICP-AES) to confirm the presence of βGP-Na and GP-Ca in release media and HA release while polymer/HA composite degradation. Films weighed about 50 mg were soaked in 10 mL PBS (pH 7.4) solution and incubated at 37 °C. At every week, the degradation media of each sample were harvested and the 10 mL PBS (pH 7.4) solution was replenished for future degradation. The degradation media was

mixed with 10 wt. % HNO_3 solution in 1:1 ratio for ICP-AES sample preparation. The released calcium concentration was read directly from ICP-AES report[38] and the released phosphorus concentration was calculated by subtracting the phosphorus concentration of blank PBS read from ICP-AES report.

2.2.8 Tensile Mechanical Tests

Tensile tests of polymer films were conducted on an Instron 5966 machine equipped with a 500 N load cell. Samples were cut into rectangle strips and pulled until failure at a speed of 500 mm min^{-1} to obtain stress–strain curves. The initial slope (0–10%) of the stress–strain curve was used to determine the initial modulus of each sample. Six specimens were averaged for each sample, and the results were presented as means ± standard deviation.

2.2.9 Morphology study by SEM

To observe morphology of microparticle scaffolds and differentiating hMSCs, scanning electron microscopy (SEM, Zeiss Sigma) were used to capture and analyze images at 10 kV. All the samples were coated with 5 nm iridium using Leica sputter coater before imaging.

2.2.10 Mass Spectroscopy

The averaged molecular weight and PDI were calculated from the full spectra or the spectra with low mass cut-off at m/z 300 as specified in the figure. M_n was calculated by Equation 1:

$$\bar{M}_n = \frac{\Sigma n_i M_i}{\Sigma n_i} = \frac{\Sigma c_i}{\Sigma\, c_i / M_i}$$ **Equation 1**

M_w was calculated by Equation 2:

$$\bar{M}_w = \frac{\Sigma n_i {M_i}^2}{\Sigma n_i M_i} = \frac{\Sigma c_i M_i}{\Sigma c_i}$$ **Equation 2**

The Polydispersity index (PDI) was calculated by Equation 3:

$$PDI = \bar{M}_w / \bar{M}_n$$ **Equation 3**

Here n_i is the number of molecules with molecular weight of M_i, which is calculated by peak area of M_i in mass spectra; c_i is the weight concentration of molecules with molecular weight of M_i; M_i is the molecular weight read from each peak in the spectra. The peak area was only integrated into averaged molecular weight calculation when the peak height is 1.5 times higher than the baseline.

2.3 Results and Discussion

2.3.1 POC, POC-βGPNa and POC-GPCa are incorporated into citrate-based materials

To verify the successful incorporation of functional monomers into the citrate-based polymer system, POC-βGP-Na and POC-GP-Ca were selected as two representatives for chemical structure tests, mechanical tests and contact angle measurement due to their high value in bone regeneration applications as mentioned in Chapter 3. The synthesis of POC-GP is similar to that for POC through a one pot polycondensation of citric acid, 1,8-octanediol and βGP-Na/GP-Ca to obtain the POC-βGP-Na/POC-GP-Ca pre-polymers,

which can be further crosslinked (post-polymerization) to prepare polymer films (**Figure** 2.1). It should be noted that after the pre-polymer syntheses, both POC-βGP-Na/POC-GP-Ca pre-polymers were purified via dialysis followed by freeze-drying to remove soluble and unreacted monomers. All the investigated formulations of the POC-βGP-Na and POC-GP-Ca in the present study are listed in **Table 1**.

Next, the chemical structures of POC and POC-βGPNa were determined by ^{31}P NMR and FT-IR spectroscopy. In ^{31}P NMR spectra (**Figure** 2.1), the peak at -1.19 ppm was assigned to phosphate triester group (PO_4^{-3}) from βGPNa while no peak was shown in the spectrum of POC, indicating the successful incorporation of βGPNa in POC-βGPNa pre-polymer through the one-pot polycondensation reaction. In FT-IR (**Figure** 2.1), the strong peak at 1705 cm^{-1} was assigned to the ester group (-C(=O)OR), the broad peak at 2932 cm^{-1} was from methylene groups in 1,8-octanediol, and the broad band at 3470 cm^{-1} represented hydroxyl groups (-OH). The band at 1194 cm^{-1} as shown in POC indicated stretch vibration of C-O in ester group. Due to the electron coupling between phosphate and carboxyl group, the peak of C-O shifted to a lower wavelength number (1170 cm^{-1}) in POC-βGP-Na and POC-GP-Ca [39]. The FT-IR results further confirmed the successful synthesis of POC-βGPNa and POC-GPNa.

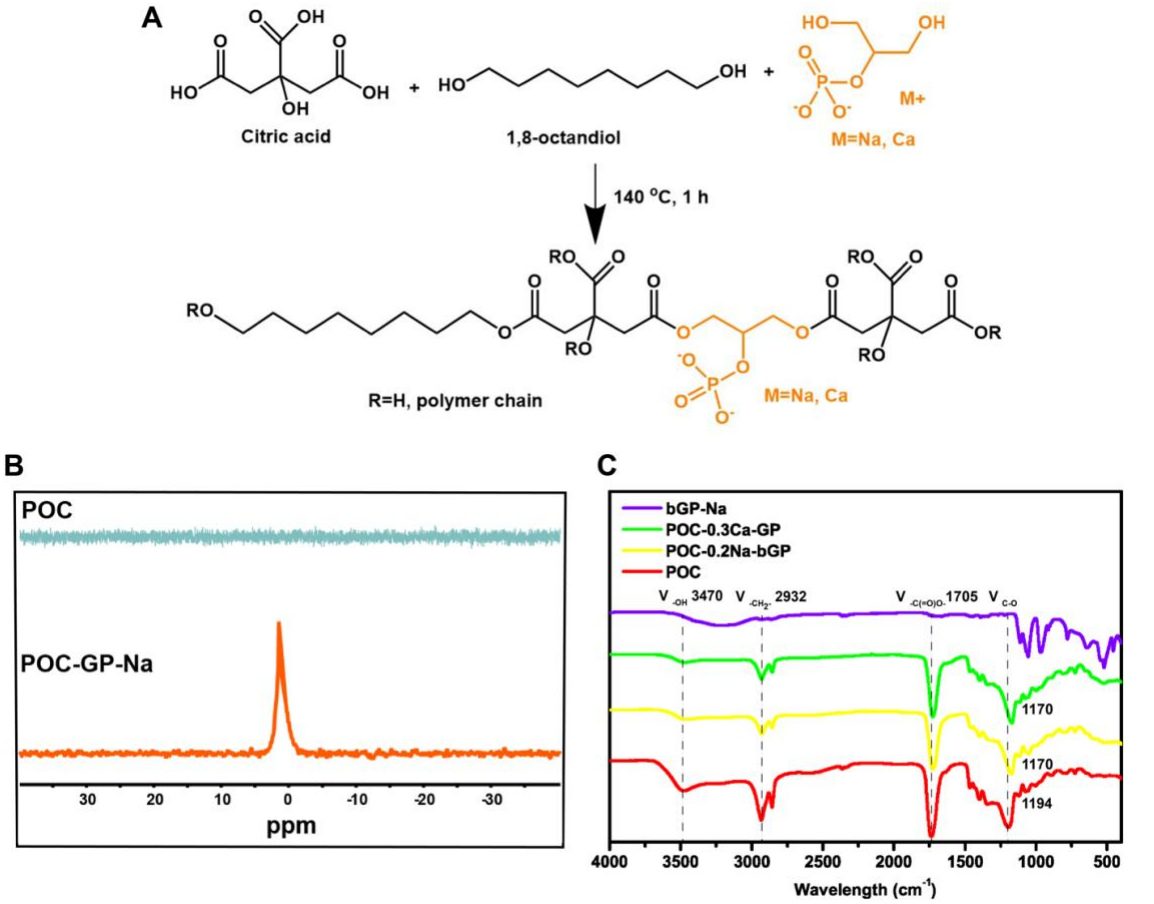

Figure 2.1 Synthesis and Characterization of POC-GP polymers. (**A**) Schematic representation of POC-GP pre-polymer synthesis. (**B**) ^{31}P-NMR analysis of the POC-GP polymers. (**C**) FT-IR analysis of POC-GP pre-polymers.

2.3.2 GP incorporation improved mechanical strengths

Next, we performed tensile mechanical tests on both POC-βGPNa and POC-GPCa polymer films (**Figure** 2.2 & **Table 2**). For POC-GPNa, its mechanical properties were significantly affected by the feeding ratio of βGPNa, evidenced by the tensile stress-strain curves (**Figure** 2.2), in which POC-0.2βGPNa and POC-0.3βGPNa displayed classical stress-stain curves of elastomers similar to POC, while POC-0.5βGPNa showed a curve of plastic

deformation. More importantly, by increasing the hydrophilic βGPNa content, the initial tensile modulus was increased about 72 times from POC (3.55±0.35 MPa) to POC-0.5βGPNa (256.44±22.8 MPa), and the tensile strength was elevated about 11 times from POC (2.5±0.18 MPa) to POC-0.5βGPNa (28.2±2.44 MPa). More importantly, the introduction of GPCa into POC could further improve the material's mechanical strengths, as shown in **Figure** 2.2 that POC-0.3GPCa (22.76±1.06 MPa) exhibited significantly higher tensile strength than the POC-0.3βGPNa (13.36±3.77 MPa). By changing the GP salt type during synthesis, the initial tensile modulus was increased (**Table 2**) about 9 times from POC-0.3βGPNa (5.81±0.11 MPa) to POC-0.3GPCa (55.08±9.68 MPa), probably due to the improved polymer crosslinking between ionic calcium and the citrate polymer networks. These above results demonstrated the addition of GP salts and choice of GP salts could be adopted as a convenient way to modulate the mechanical properties of the resultant citrate polymers. Also, the tensile strengths of the resultant POC-GP polymer films without HA reinforcement ranging from 5.28±0.56 MPa to 28.20±2.44 which are similar to that of natural skin (1-20 MPa) and within the range of articular cartilage (9-40 MPa) [40], suggesting that the mechanically tunable POC-GP polymers may have a potential to be applied in different tissue applications.

Table 2 Improved mechanical properties of the POC-GP crosslinked polymer films in comparison with POC.

	Initial's Modulus (MPa)	Tensile strength (MPa)	Elongation (%)
POC	3.55±0.35	2.50±0.18	144±28
POC-0.2βGP-Na	5.28±0.56	7.45±1.63	270±52
POC-0.3βGP-Na	5.81±0.11	13.36±3.77	361±34
POC-0.5βGP-Na	256.44±22.88	28.20±2.44	15.7±4.2
POC-0.2GP-Ca	10.65±2.65	13.06±0.59	182±26
POC-0.3GP-Ca	55.08±9.68	22.76±1.06	199±7.0

Thermo-crosslinking conditions: 3 days at 80°C and 1 day at 120°C under vacuum

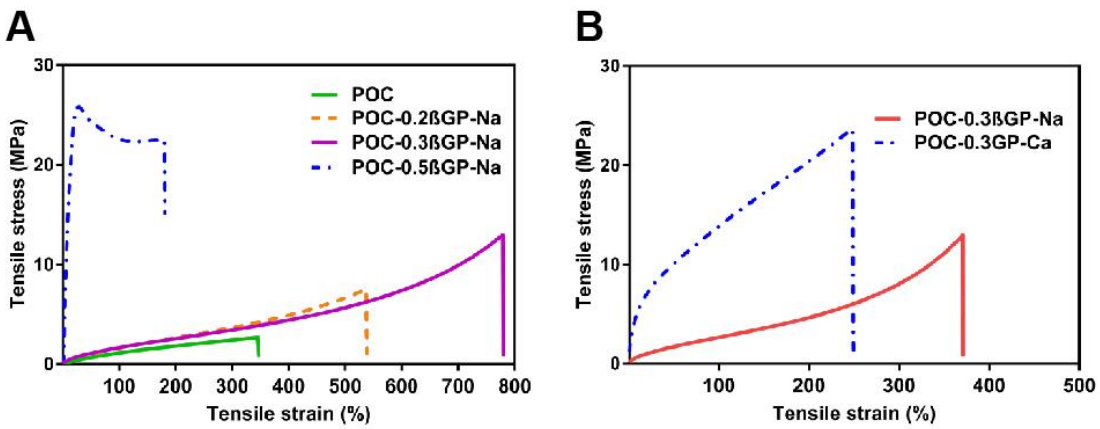

Figure 2.2 Mechanical properties of POC-GP films. (**A**) Stress-strain curves of POC, POC-0.2βGPNa, POC-0.3βGPNa, and POC-0.5βGPNa polymers. (**B**) Stress-strain curves of POC-0.3GPCa in comparison with POC-0.3βGPNa.

2.3.3 Contact angle and mass loss study

The mass loss studies of these 5 representative citrate-based polymers or polymer composites demonstrated the degradation performance in a macroscopic way and revealed that the degradation rate was closely related to polymer formulation as shown in **Table 1**. Overall, the mass loss curves of all polymer/HA composites and polymer films showed the same trend: a slower increase at earlier times (1-2 weeks) and a faster increase followed thereafter until 12 weeks. For pure polymers, POC exhibited the slowest degradation, with a 82% remaining mass at 8 weeks in PBS at 37°C , while POCX exhibited the fastest degradation, with almost 50 wt% mass loss in the same time frame, as shown in **Figure** 2.4. In comparison, the PHC film showed a faster degradation than POC film because the 1,6-hexanediol in PHC has a lower hydrophobic alkane content than the alkane content in 1,8-octanediol in POC. Additionally, it is obvious that POC-GP-Na and POC-GP-Ca degraded fast but slower than POCX, due to the lower hydrophilicity and lower content of added monomers. The POC-GP-Ca showed a faster mass loss rate than POC-GP-Na can be explained by the same reason[38, 41].

In

Figure 2.3, a final remaining mass of polymer/HA composites at 12 weeks were 63% - 95% when the degradation was ceased at 12 weeks which is much slower than pure polymer films with a 52% - 82% mass loss at 8 weeks. In comparison, the degradation rate between 5 citrate-based/HA composites showed a very similar trend to their pure polymers. However, there were no significant differences in weight loss between PHC/HA composites and POC-GP-Na/HA composites.

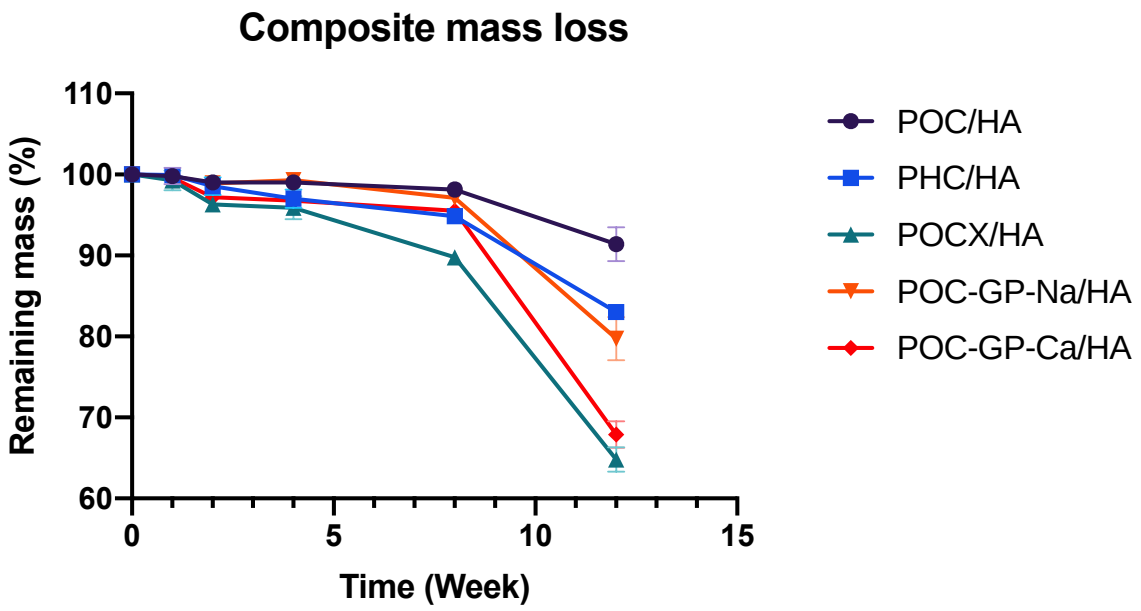

Figure 2.3 Degradation of POC/HA, PHC/HA, POCX/HA, POC-βGPNa/HA, and POC-GPCa/HA polymer composites measured by mass loss in PBS in 12 weeks.

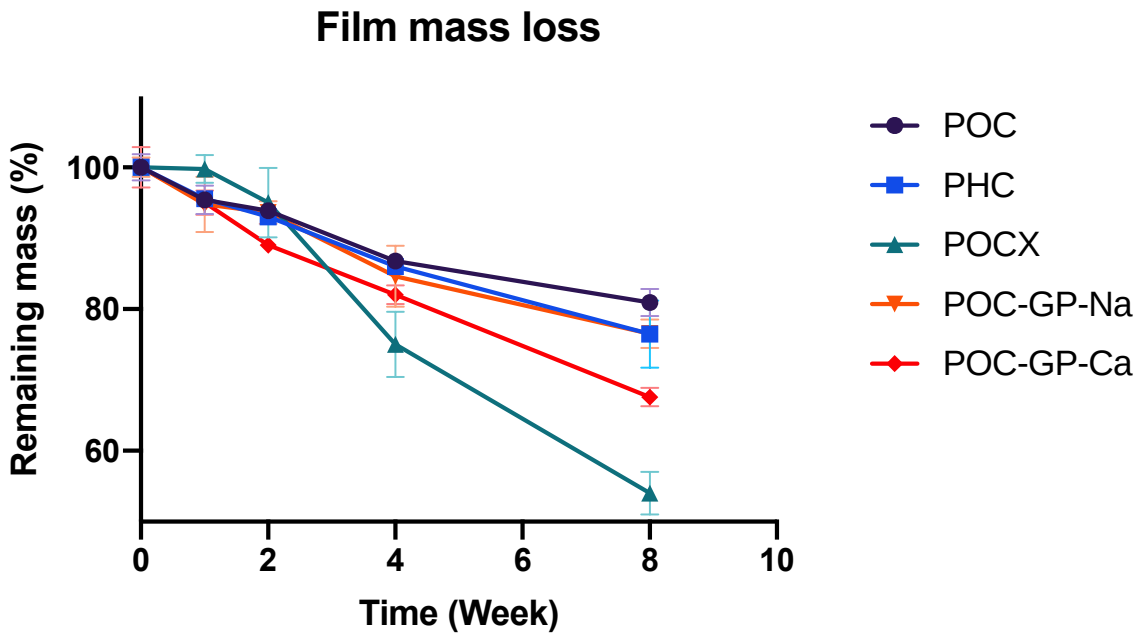

Figure 2.4 Degradation of POC, PHC, POCX, POC-βGPNa, and POC-GPCa polymer films measured by mass loss in PBS in 8 weeks.

Considering the material's degradation may affect cell responses, tissue penetration and the life-span of the implants [42], we sought to screen the *in vitro* degradation rate of different polymers in an accelerated manner in 0.05 M NaOH. In order to tune the material degradation, the monomer ratios of βGPNa over citric acid were varied. Interestingly, degradation studies in phosphate buffered saline (PBS) showed that the increase of βGPNa content from 0.2 to 0.3 in POC polymer networks accelerated the degradation rate **Figure** 2.5 **A**, but further increase of the GPNa molar ratio (POC-0.5βGPNa) resulted in slower degradation as compared with that of POC. As suggested in **Figure** 0.1 **A**, adding GP salts into POC slightly improved the wettability resulting in faster degradation of POC-0.2βGPNa over POC. However, increasing βGPNa in POC resulted in the loss of elasticity,

especially for POC-0.5βGPNa that might become semi-crystalline **Figure** 2.2, leading to slower degradation. For accelerated degradation as shown in **Figure** 2.5 **B**, POC-βGPNa and POC-GPCa all showed a faster degradation speed than POC in 0.05 M NaOH suggesting that adding GPs significantly affect the degradation of the resultant polymers. The accelerated degradation data were also in agreement with the contact angle data showing that POC-βGPNa and POC-GPCa have similar wettability but more hydrophilic than POC. Overall, the degradation of POC-GP was expected to be multifaceted and can be tuned by the hydrophilicity of monomers, monomer feeding ratios, and polymer chain length from this paper and our previous study [43-44].

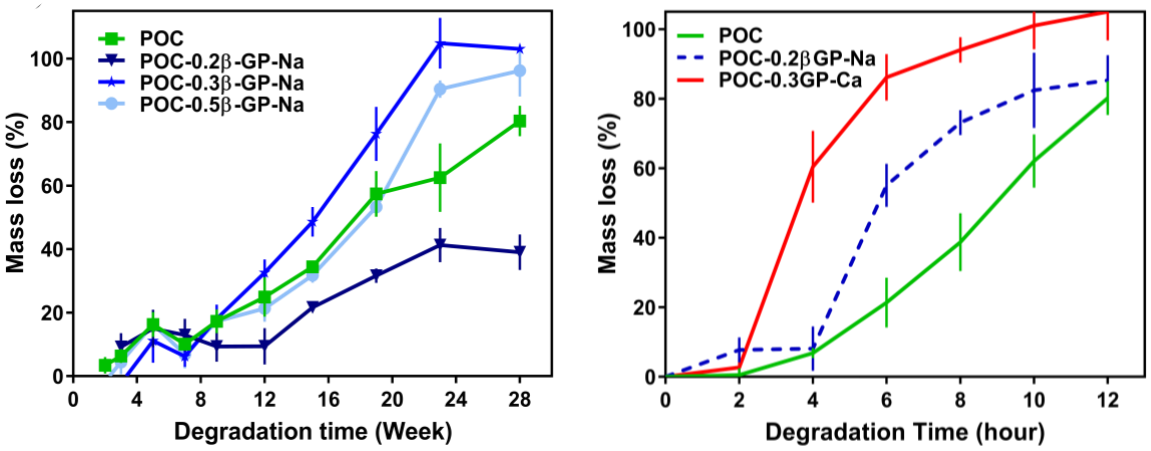

Figure 2.5 (**A**) Degradation of POC and POC-βGPNa polymer films in PBS (**B**) Accelerated degradation of POC, POC-0.2βGPNa and POC-0.3GPCa polymer films in 0.05M NaOH.

The wettability of POC-GP films was also evaluated as representatives among 5 citrate-based polymers by water-in-air contact angle tests using POC as control. As shown

in **Figure** 2.6, the contact angle of both POC-βGPNa and POC-GPCa was lower than that of POC initially, but it became close to that of POC after 60 s, indicating the hydrophilic nature of POC-GP backbones with similar wettability to POC.

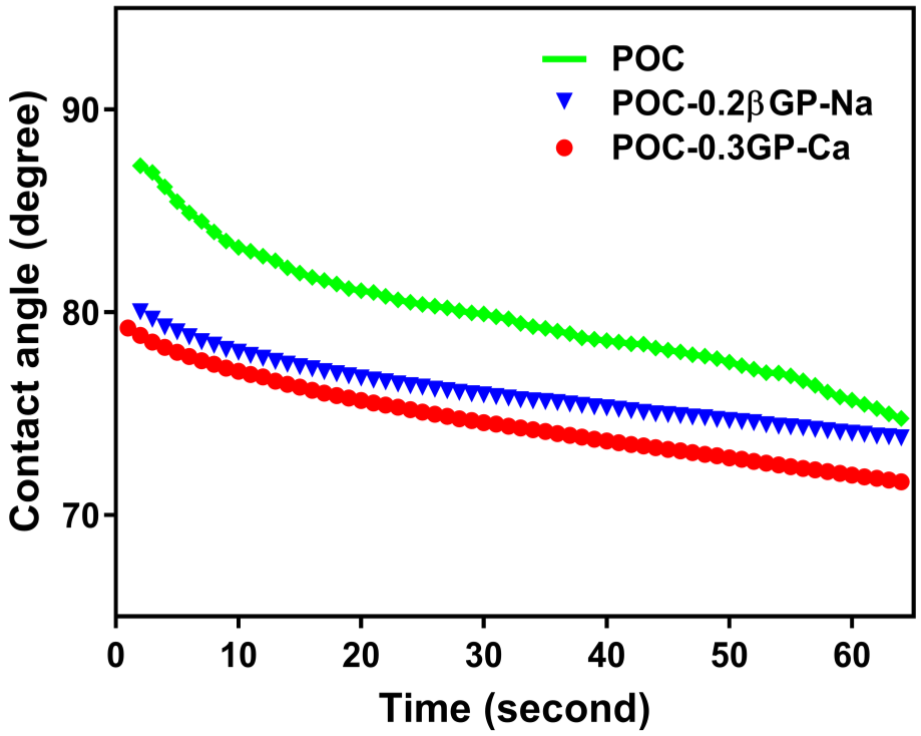

Figure 2.6 Contact angle changes over time tested on the POC-0.2βGPNa and POC-0.3GPCa crosslinked polymer films.

2.3.4 Molecular weight and PDI characterization from Mass spectroscopy

It is widely known that a polymer's molecular weight can decrease due to chain scission during degradation [45-46]. GPC and MALDI-MS are usually utilized to facilitate monitoring of polymer molecular weight changing. **Figure 2.8** lists the series of mass spectra obtained

from POC/HA composites degradation products on week 1, 2, 4 and 8. All of them includes intensive molecule ion peaks of [$C_6H_6O_7$-CO_2-H_2O-H]- at m/z 129 and peaks distributed among m/z 100 to 2000. The averaged molecular weight and PDI were calculated from the full spectra or the spectra with low mass cut-off at m/z 300 as specified in the Chapter 2.2.10 and the peak area was only integrated into averaged molecular weight calculation when the peak height is 1.5 times higher than the baseline.

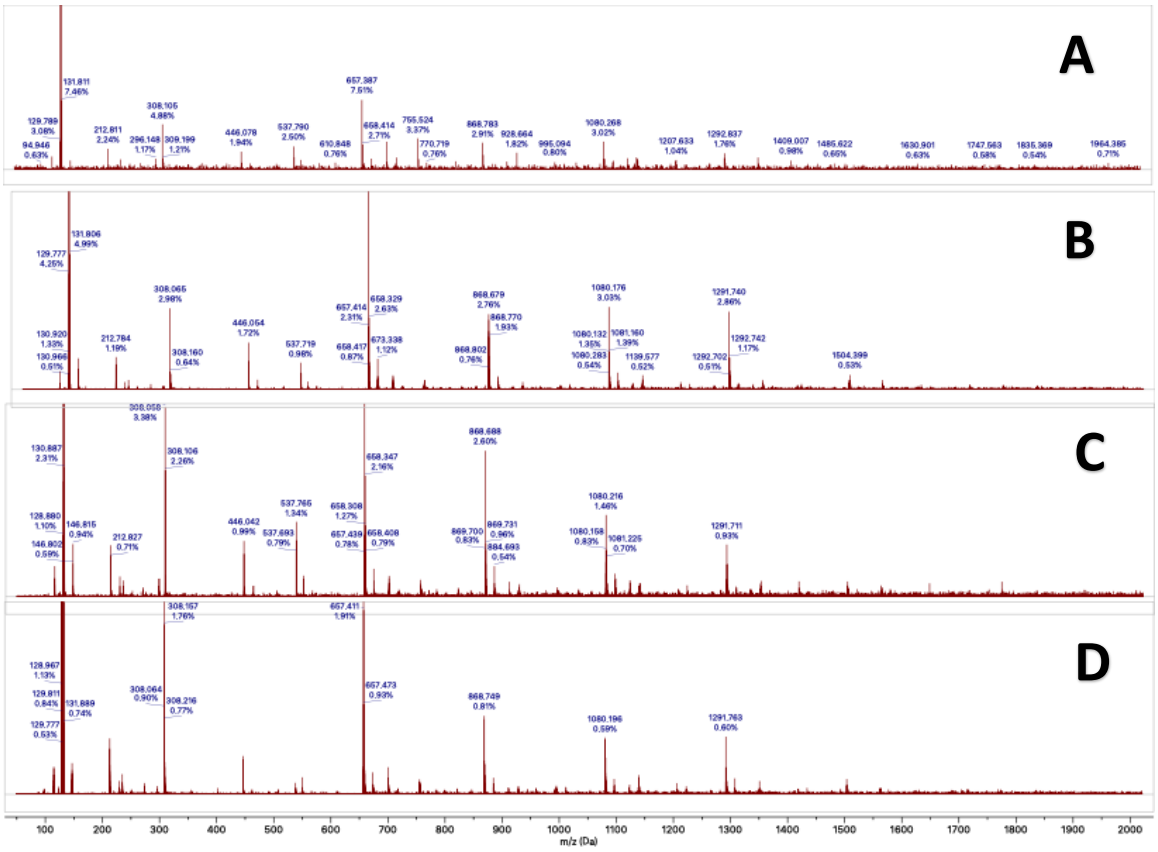

Figure 2.7 MALDI-MS spectra of POC/HA degradation products from (A) week 1, (B) week 2, (C) week 4, and (D) week 8.

Figure 2.8 and **Figure 2.10** shows the change in Mn of POC/HA, PHC/HA, POCX/HA, POC-0.2βGPNa/HA and POC-0.3GPCa/HA composites from full spectra and the spectra with a low mass cut-off at m/z 300. Mn from both spectra showed increased molecular weights from week 1 to week 2, and the Mn decreased throughout week 2 to week 8 for all 5 polymer composites. Generally, in full spectra, the averaged molecular weight of different composites varies between 378 Da to 496 Da, which is in accordance of Mn of oligomers made of 2 monomers. After excluding monomer peaks from the spectra, **Figure 2.10** showed a similar trend as Figure 2.9 while the Mn ranges from 881 Da to1063 Da. This Mn range fits the molecular weight characterization of citrate-based pre-polymers from previous studies. Combining Figure 2.9 and Figure 2.10 together, we can infer that unreacted monomers, cleaved oligomers, and pre-polymers were released from bulk polymer composites during degradation, which happened to all 5 citrate-based polymers mentioned in this study. However, it's challenging to tell if the detected monomers were leached from bulk scaffolds or cleaved from polymer chains by hydrolysis.

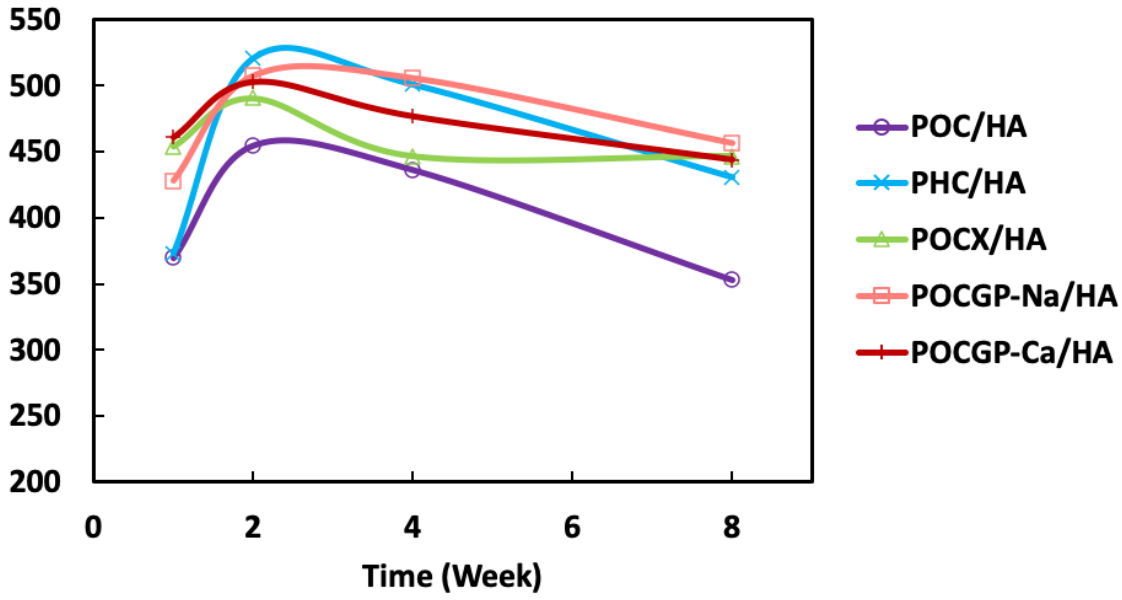

Figure 2.8 Number average molecular weight (Mn) of polymer composites degradation products from full spectra of MALDI-MS.

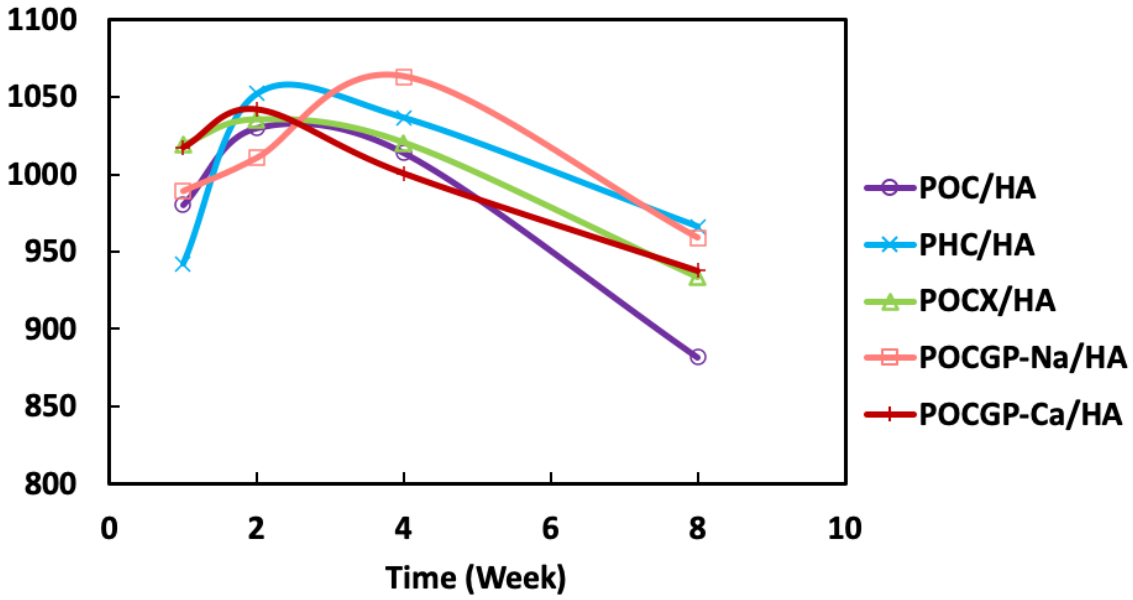

Figure 2.9 Number average molecular weight (Mn) of polymer composites degradation products from MALDI-MS with a low mass cut-off at m/z 300.

Figure 2.10 and **Figure 2.12** shows the change in PDI of these composites. During the 8 weeks incubation time in PBS 7.4, calculated from full spectra and the spectra with low mass cut-off at m/z 300. In **Figure 2.11**, the PDI dropped significantly after composites degraded for 2 weeks, while PDI in **Figure 2.12** remained the same with time. Based on the fact that all the monomer peaks were taken into consideration for PDI calculation in Figure 2.11, the decreased PDI within the first two weeks indicates there may be some unreacted monomers released and the PDI remained relatively constant after 4 weeks as more oligomer-sized fragments released from the polymers due to degradation. While in Figure 2.12 (mass cut-off at m/z 300), the PDI remained constant throughout the degradation period suggesting that polymers degraded and released prepolymer or oligomer-sized species since monomer-sized species were excluded.

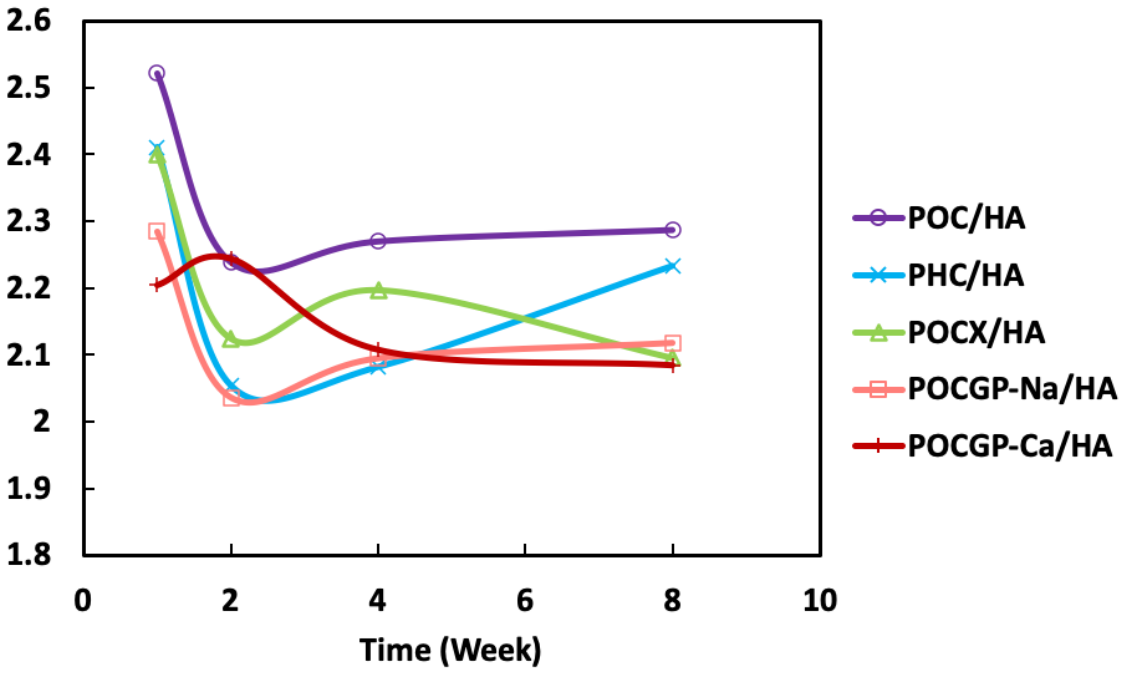

Figure 2.10 Polydispersities (Mw/Mn) of polymer composites degradation products from MALDI-MS.

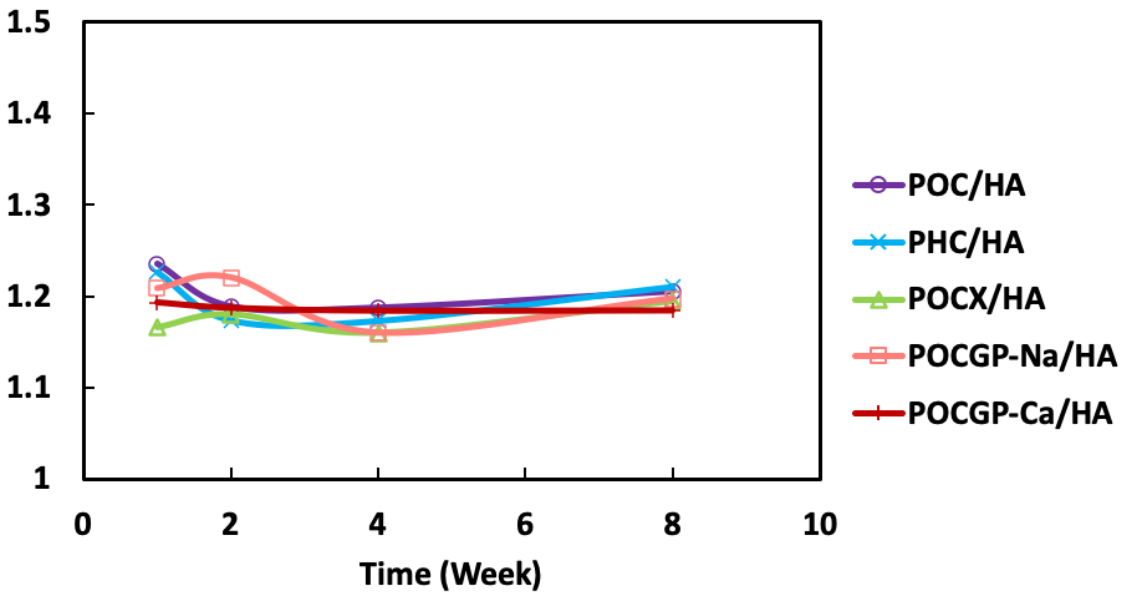

Figure 2.11 Polydispersities (Mw/Mn) of polymer composites degradation products from MALDI-MS with a low mass cut-off at m/z 300.

2.3.5 Phosphorus and calcium release

Further, ICP-AES revealed the accumulative release of phosphorus and calcium from POC/HA, PHC/HA, POCX/HA, POC-βGPNa/HA, and POC-GPCa/HA composites during degradation in PBS.

For calcium release from polymer/HA composites, in **Figure** 2.12, calcium concentration which gradually increased from 1.1 mg/L to 5.8 mg/L, and 2.2 mg/L to 21.3 mg/L for POC-βGPNa and PHC, respectively, ranking the slowest and fastest among these 5 polymer/HA composites. The trend and ranks among all these candidates are completely different from the mass loss trend during degradation and it may be explained by the various binding force between hydroxyapatite and polymers existing in the composites [18]. In **Figure** 2.13, while POC/HA showed a slow increase phosphorus release through 12

weeks degradation, PHC/HA, POCX/HA, POC-βGPNa/HA, and POC-GPCa/HA demonstrated a decrease along time. Previous research illustrated citrate enhanced phosphorus absorption, explaining the reduction of phosphorus in solution with time [47]. The above results suggest that citrate polymer/HA composites may act as both the sources of phosphorus initially but may also help absorbing or contenting phosphorus at later times depending on formulations.

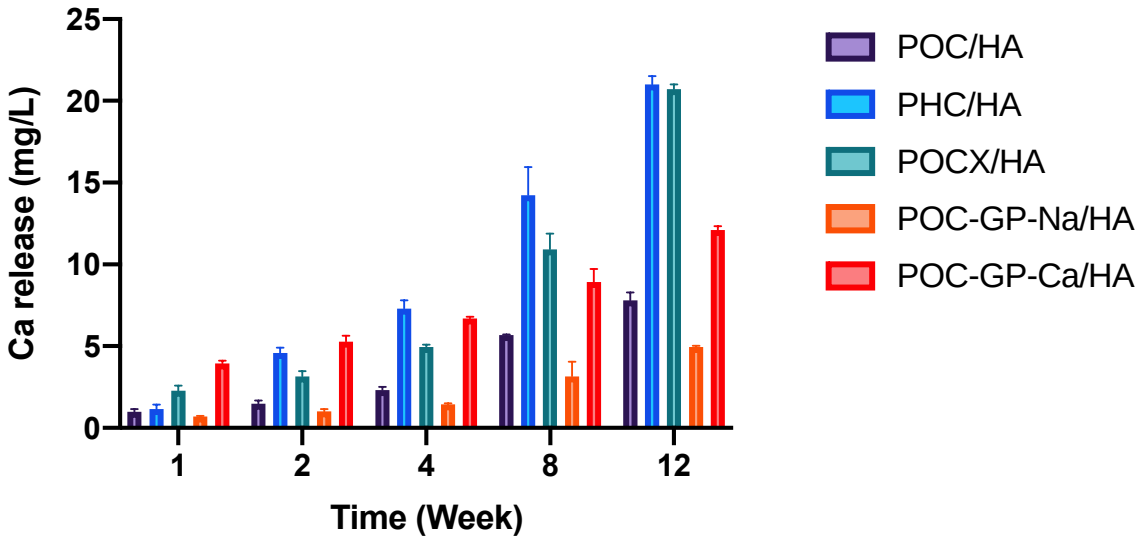

Figure 2.12 Accumulative release of calcium from POC/HA, PHC/HA, POCX/HA, POC-0.2βGPNa/HA and POC-0.3GPCa/HA composites.

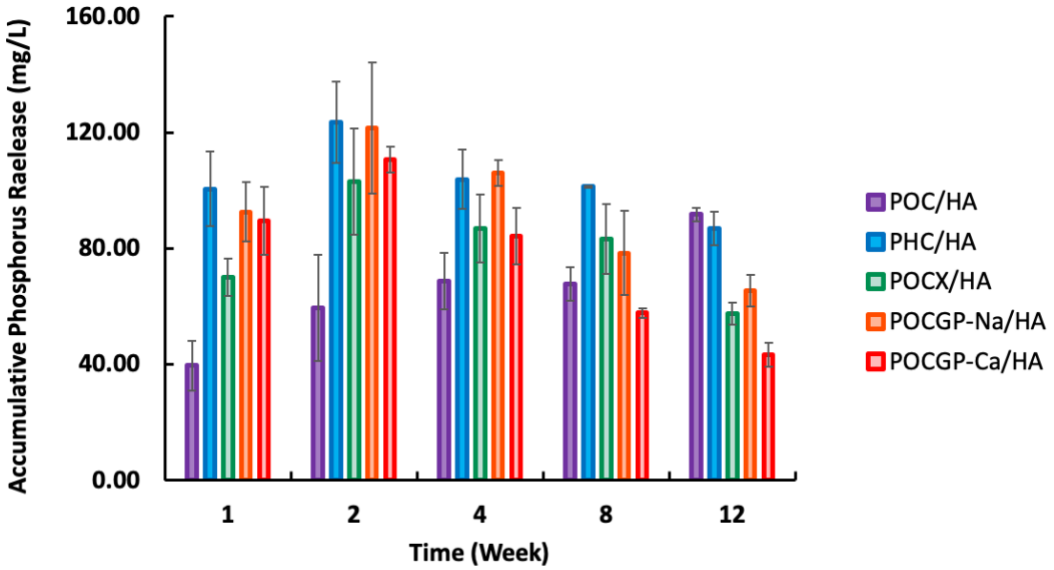

Figure 2.13 Accumulative release of phosphorus from POC/HA, PHC/HA, POCX/HA, POC-0.2βGPNa/HA and POC-0.3GPCa/HA composites.

As reported, there're many factors which could affect the degradation and release process of citrate-based polymers or composites, such as pre-polymer formulations, pre-polymer functional groups, the crosslinking conditions, and fabrication methods of scaffolds. Together with our previous finding that citrate as an osteopromotive factor, antibacterial factor, chelating agent and etc., the sustainable release of citrate and other functional monomers from citrate-based polymers is necessary for the aimed application. Thus, the above phosphorus and calcium release results strongly suggested that the citrate-presenting polymers doped with bGP-Na, GP-Ca, xylitol and other additional monomers hold great potential to function as an expected resource of organic phosphorus or calcium in different biomedical engineering applications, especially bone regeneration. The release

of phosphorus and calcium, existing in hydroxyapatites and glycerophosphate, and the mass loss from pure polymer films can also indirectly prove that citrate was set free during degradation. Future characterization of citrate release with the assist of HPLC will further confirm this hypothesis.

2.4 Conclusion

The degradation rate and release profile *in vivo* usually largely affect the biodegradable materials' performance in tissue engineering field. Thus, the comprehensive understanding of polymer chain structures after degradation can give rise to an accuracy prediction of pure polymers, polymer blends and polymer composites properties based on the structure-property connections.

As one of the trendiest biodegradable polymer families, citrate-based polymeric biomaterials gained its popularity in tissue engineering, drug delivery, food processing and many other related applications. In this chapter, citrate-presenting polymers doped with bGP-Na, GP-Ca, xylitol and other functional monomers were thoroughly characterized in term of chemical structure, mechanical properties, hydrophilicity/hydrophobicity, and their degradation behaviors. Using POC as a control, contact angle data showing that POC-βGPNa and POC-GPCa have similar wettability but more hydrophilic than POC, in accordance of the degradation profile. The mechanical properties of citrate-based polymers were able to be tuned by different types of monomers and monomer feeding ratios from this paper and our previous study [43-44]. The phosphorus and calcium release results strongly suggested that the citrate-presenting polymers or composites hold great potential to

function as an expected resource of organic phosphorus or calcium in different biomedical engineering applications, especially bone regeneration. The release of phosphorus and calcium, existing in hydroxyapatites and glycerophosphate, and the mass loss from pure polymer films can also indirectly prove that citrate was set free during degradation. Future characterization of citrate release with the assist of HPLC will further confirm this hypothesis. Herein, this study established a concrete understanding on the chemical and physical properties of the citrate polymers and their composites, providing a comprehensive guidance and reference for future applications such as bone regeneration.

3 Chapter

DEVELOPMENT OF OSTEOPROMOTIVE POLYESTER FOR ENHANCED BONE REGENERATION

3.1 Introduction

Over 2.2 million bone grafting procedures performed annually worldwide [43] in orthopedics, neurosurgery and dentistry surgeries. Bone substitutes are increasingly needed and applied in those surgeries. The development of fully synthetic bone substitutes, that are readily available, cost-effective, and osteogenesis-supportive, is particularly encouraged in the clinical field [48]. Despite all the progress, the currently available synthetic materials are limited by their inabilities to mimic the native tissue composition, weak mechanical strength, significant inflammatory responses, poor bone integration, and slow bone regeneration [49]. Inspired by natural bone, the native biocomposite comprised of collagen as the major organic component providing the naturally derived polymeric framework for the inorganic calcium phosphate (CaP) minerals to grow on, inorganic bioceramics, such as hydroxyapatite (HA), and tricalcium phosphate (TCP), have been introduced into the biodegradable synthetic polymers to create biomimetic composites aimed at better resembling the native bone composition [50-53].

Citrate, the molecule highly accumulated in natural bone, has been found to strongly bind to bone inorganic minerals, playing indispensable roles in stabilizing the mineral crystals [54] and controlling the crystal size [19]. As a robust multifunctional monomer,

citrate chemistry enables the formation of a 3D cross-linked network structure when reacted with different diols [12, 16]. Meanwhile, it provides rich pendant carboxyl and hydroxyl groups to allow the incorporation of up to 65% weight of HA, closely resembling the inorganic composition of natural bone. During the past decade, a series of citrate-based materials/HA composites have been developed in our lab and have demonstrated impressive *in vivo* performance in various animal models for bone regeneration, such as poly(octamethylene citrate)/HA (POC/HA) for osteochondral defect healing (in rabbits) [55], clickable POC/HA (POC-click/HA) for long segmental radial bone regeneration (in rabbit) [56] and for cranial defect repair (in rats) [57], citrate-based polymer blends/HA (CBPB/HA) for the repair of lateral femoral condyle defect (in rabbits) [58], injectable citrate-based mussel-inspired tissue bioadhesives/HA composite (iCMBA/HA) for comminuted radial bone regeneration (in rabbits) [59], as well as N-methyldiethanolamine (MDEA) modified click-crosslinked POC-click/HA (POC-M-click/HA) for spinal fusion (in rabbits)[60]. Excitingly, one of our recent studies[18] demonstrated that citrate released from our materials could promote the differentiation of human mesenchymal stem cells (hMSCs) towards active bone forming cells by regulating energy-producing metabolic pathways. The newly discovered citrate metabonegenic regulation mechanism not only highlights the significance of citrate-based composites for orthopedic applications, but also provides valuable guidance to design materials with improved osteo-promotive functionality. For example, phosphoserine, the native organic phosphate donor in bone, when incorporated in citrate polymers or in its solute form, was found to play concerted action with citrate leading to accelerated bone formation and maturation [18]. The above studies suggested phosphoserine could synergize with citrate to further promote osteogenic differentiation of

hMSCs. It points to a direction in designing citrate-based biomaterials by carefully selecting appropriate molecules to construct polymers with citrates for further improving osteo-promotive functionality.

Mechanical properties are also an important factor of materials that greatly affect tissue engineering efficacy, especially for bone repair, in addition to a material's potential of supporting osteogenesis[61]. Numerous efforts have been made in our lab to improve the mechanical properties of citrate-based materials, especially for orthopedic applications. The introduction of urethane groups into citrate-based polyester materials has been proved to be an effective way of improving mechanical strength but sacrifices the valuable pendant groups for further biofunctionalization and HA chelation [57, 62]. Clickable biodegradable elastomer, employing click chemistry as an additional crosslinking mechanism, has also shown with robustly improved mechanical property, while displaying a delayed degradation rate compared with POC, making it unsuitable for applications requiring fast-degrading scaffolds [60, 63]. The relatively complex click-monomer synthesis also makes the click-polymers less attractive. Therefore, balancing the mechanical properties and biodegradation rate while introducing biofunctionality into polymer networks in a more convenient way remains as a challenge.

β-glycerophosphate disodium (βGPNa), widely known as an osteogenic medium supplement and a weak base, has been used to initiate the gelation of chitosan or collagen to generate thermosensitive injectable hydrogels[20]. Another GP salt, glycerophosphate calcium (GPCa), representing as a mixture of β-isomer (80%) and rac-α-isomer (20%), has long been used as food supplement for both calcium and phosphate. Given the osteopromotive benefits of both salts in their solute and conjugated form [21-23], we

incorporated two types of GP salts into the citrate-based materials through a one-pot polycondensation reaction by taking advantage of the reactive nature of citric acid, to prepare POC-GP, in order to further improve the bioactivity of citrate materials to promote stem cell osteogenic differentiation. At the same time, our results show that GP incorporation greatly increased the mechanical properties of the resultant polymer. By changing the salt type and feeding ratio and polymerizing the monomers in a very convenient, one-pot polycondensation, the degradation rate of the resulting polymers can also be easily tuned, providing an alternative way to balance mechanical properties, degradation, and bioactivity. A rabbit femoral condyle defect model was used to evaluate the efficacy of POC-GP/HA for bone regeneration. It was observed that the osteopromotive capabilities of GP-doped POC were significantly improved compared with POC and autograft control groups.

3.2 Experimental section

3.2.1 Sample preparation

Polymer films and polymer/HA composites used in the cell study and animal study below were prepared as described in Chapter 0. The pre-polymer made for bone regeneration promotive implants were synthesized according to the formulation in

Table 3. The dried pre-polymer was then thermally crosslinked at 80°C for 3 days and then at 120°C with vacuum for 1 day to obtain a stronger crosslinked polymer film.

To prepare the polymer/HA microparticles, porous composite scaffolds were first prepared by mixing pre-polymer solution, HA and NaCl salts at the size of 250-425 μm

before casted flat in Teflon dishes. After the solvent evaporated, the scaffolds were thermally crosslinked and then soaked in de-ionized (DI) water to leach the salt. Next, the porous sponge-like scaffolds were freeze-dried, grinded and sieved into different sizes of microparticle scaffolds (<150 μm; 150-250 μm; 250-425 μm; >425 μm).

Table 3 Formulations of pre-polymer synthesis

	Citric acid (M)	1,8-Octandiol (M)	βGP-Na or GP-Ca (M)
POC	1.0	1.1	/
POC-0.2βGP-Na	1.0	0.9	0.2
POC-0.3βGP-Na	1.0	0.8	0.3
POC-0.5βGP-Na	1.0	0.6	0.5
POC-0.2GP-Ca	1.0	0.9	0.2
POC-0.3GP-Ca	1.0	0.8	0.3

3.2.2 Phosphorus release studies

Accumulative phosphorus release content was investigated by inductively-coupled plasma emission spectroscopy (ICP-AES) to confirm the presence of βGPNa and GP-Ca in release media. Films weighed about 50 mg were soaked in 10 mL PBS (pH 7.4) solution and incubated at 37 °C. After 14, 21, and 28 days, release media of each sample were mixed with 10 wt. % HNO_3 solution in 1:1 ratio for ICP-AES sample preparation. The released phosphorus concentration was read directly from ICP-AES report.

3.2.3 Morphology of microparticle scaffolds and hMSCs

To observe the morphology of microparticle scaffolds and differentiating hMSCs, scanning electron microscopy (SEM, Zeiss Sigma) was used to capture and analyze images at 10 kV. All the samples were coated with 5 nm iridium using Leica sputter coater before imaging.

3.2.4 Cell culture

In vitro cell studies were performed with human mesenchymal stem cells (hMSCs) in passage 5-7. Growth media (GM) were composed of Dulbecco's Modified Essential Medium (DMEM) supplemented with 10% fetal bovine serum and 100 units/mL of penicillin-streptomycin. Osteogenic media (OG) were composed of growth media supplemented with 0.2 mM ascorbic acid, 50 nM dexamethasone, and 10 mM β-glycerophosphate disodium. Solid samples were submerged in 70% ethanol for 1 hour and sterilized by UV irradiation for 1 hour on each surface. For liquid samples, solutions were sterilized by filtering through sterile syringe filter (0.2 μm cellulose acetate, VWR, PA). For all cell studies, cells were kept in a humidified incubator at 37℃ with 5% CO_2. Both GM and OM were replaced every other day.

3.2.5 In vitro cytocompatibility evaluation

The cell seeding densities were 5000 cells/cm_2 and 3000 cells/cm_2 for cell cytotoxicity and cell proliferation study, respectively. At each time point, the media were removed and hMSCs were rinsed once with PBS solution. 200 uL of cell counting kit-8 (CCK-8)

solutions 1:10 diluted with culture medium, were added in each well and incubated at 37℃ for 30 minutes. The absorbance was evaluated at a wavelength of 450 nm with Tecan plate reader.

3.2.6 hMSCs differentiation study

To evaluate the hMSCs differentiation on polymer/HA composite disks and microparticle scaffolds, samples were sterilized and transferred to 48-well plates. hMSCs were seeded onto samples at a density of 3,000 cells/ cm^2 in growth media. Once cells reached 80% confluency, growth media were removed and replaced with the established osteogenic media or growth media as a general control. To evaluate the effect of GP salts concentrations on osteogenic differentiation, hMSCs were also seeded onto a 48-well plate at a concentration of 10,000 cells/mL in growth medium. Once cells reached 80% confluency, the growth media was replaced with reductive osteogenic media (DMEM with 0.05 mM ascorbate-2-phosphate, 10^{-7} M dexamethasone but without β-glycerophosphate disodium) supplemented with 0.2 mM of different GP salts.

After differentiated for 7, 14, and 21 days, cells were harvested by washing 3 times with PBS solution and lysed with 250 uL RIPA buffer for further alkaline phosphatase (ALP) assay and DNA quantification. The ALP activity was measured according to the method published previously[18]. The DNA content was tested by Pico Green dsDNA test kit according to the manufacturer's instruction. To observe the mineral and ECM formation and cell morphology on polymer/HA composites under SEM, cells were harvested and fixed in 2.5 % glutaraldehyde for 48 hours, followed by a serial dehydration process, critical-point drying, and iridium sputtering coating (Leica Sputter-coater). Gene

expression of *Runx-2* (runt-related transcription factor 2), *Col1a1* (encoding collagen type 1 alpha 1), and *SPP1* (encoding osteopontin) were evaluated by real-time PCR. Total RNA was extracted from harvested cells on day 14 with QIAGEN RNeasy kit (Hilden, Germany) and transcribed into cDNA with High-Capacity cDNA Reverse Transcription Kits (Applied Biosystems^{TM}, CA). Then real-time PCR was carried out using QuantStudio Real-Time PCR system (Applied Biosystems^{TM}, CA). The primers and TaqMan probe used for human *Runx-2*, *Col1a1*, and *SPP1* were Hs00231692_m1, Hs00164004_m1, and Hs00959010_m1.

3.2.7 Surgical procedures for animal study

An established femoral condyle defect model on New Zealand white rabbits was used for *in vivo* evaluation. according to the method described elsewhere [64-65]. Briefly, a defect with 5 mm in diameter and 5 mm in depth was created at lateral femoral condyle of each rabbit under continuous saline buffer irrigation, then the powders were filled into the defect and the musculature and skin incision were closed with nylon suture. Both the left and right condyles of femur were created per rabbit. Rabbits were randomly assigned into four groups with different bone implants in left and right legs respectively: 1) sham group (untreated); 2) POC/HA microparticle scaffold group; 3) POC-βGP-Na/HA microparticle scaffold group, and 4) POC-GP-Ca/HA microparticle scaffold group. The concentrations of HA in the composites are all 65 wt%. The particle scaffold with a mixture of different sizes were used for animal studies. After 4, 8, and 12 weeks, 4 rabbits/group were euthanized and subjected to micro-CT analyses. Then the medial femoral condyle and the

surrounding tissues were removed, fixed in 4% phosphate buffered paraformaldehyde solution, sectioned, stained for histological analysis [66]. A total of 48 New Zealand white rabbits weighing approximately 2.5 kg were used and approved by Kunming Medical University in compliance with all regulatory guidelines. The anesthesia (Pentobarbital Sodium, 30 mg/kg) for all animals was administered through marginal ear veins on the lateral aspect.

3.2.8 Micro-CT analysis

In order to quantify the new bone formation within defects, quantitative imaging of harvested femurs was performed using a micro-CT imaging system (μ-CT80 scanner; Scanco Medical AG, Brüttisellen, Switzerland) with a 3D Gaussian filter constrained at $\sigma = 1.0$ and support = 2 for partial suppression of the noise in the volumes. All the micro-CT data were processed with Mimics 21.0 software at a threshold of 2500 to discriminate new bone tissues from surrounding tissues and polymer/HA scaffold and a cylindrical region of interest (ROI) with a diameter of 5.0×3.0 mm was chosen to evaluate the newly regenerated bone. Bone volume/total volume (BV/TV) were calculated. All analyses were repeated with four specimens.

3.2.9 Histological analysis

Tissues were sectioned and fixed in 4% phosphate buffered paraformaldehyde solution for histological assessment. The sections were stained with hematoxylin and eosin (H&E) and Masson’s trichrome (Hematoxylin Staining Solution, FZ-025, Eosin Staining Solution, FZ-028, Masson's trichrome stain solution, FZ-037, Hebei Bio-High Technology Development

CO., LTD, China.) to observe the new bone formation and collagen deposition respectively within the wound areas. Digital images from each experimental group were acquired by an optical microscope in 40×, 100×, and 400× magnification

3.2.10 Statistical analysis

All quantitative data are presented as mean ± SD with a minimum of three independent samples and analyzed by one-way analysis of variance (ANOVA). P values < 0.05 were regarded as statistically significant.

3.3 Results and Discussion

3.3.1 GP release study during biodegradation

ICP-AES revealed the accumulative release of phosphorus from both POC-βGPNa and POC-GPCa polymer films during degradation in PBS, which gradually increased from 9.00±6.93 μM to 13.24±4.89 μM, and 10.41±0.84 μM to 16.53±1.74 μM for POC-βGPNa and POC-GPCa, respectively **(Figure** 0.1**)**. It indicates the possible release of GP monomers and/or inorganic phosphate from polymer films, and both GP monomers and inorganic phosphate [18] have been found to possess favorable role in bone. Together with our previous finding that citrate as an osteopromotive factor could also get released from citrate-based polymers [18], the above results strongly suggested the potential of the citrate- and GP-presenting POC-GP materials in orthopedic application.

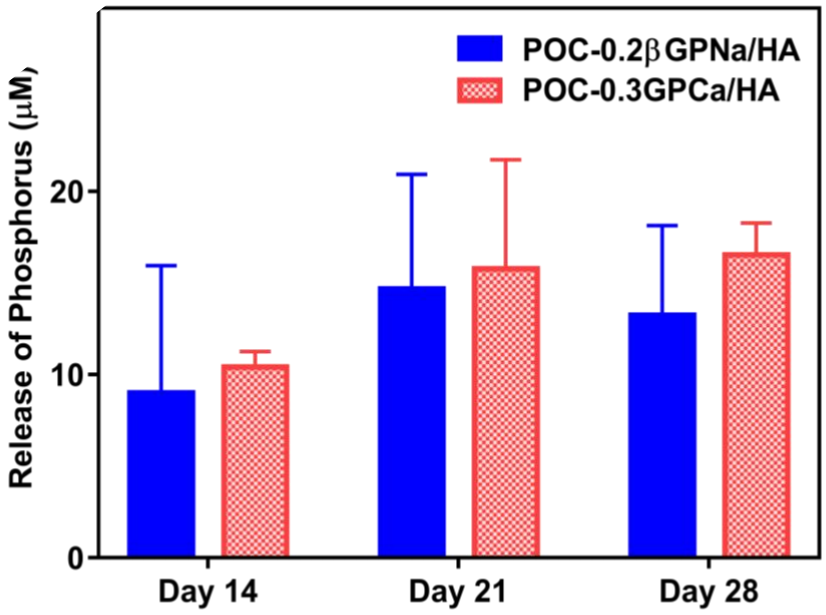

Figure 0.1 Accumulative release of phosphorus from POC-0.2βGPNa and POC-0.3GPCa films.

3.3.2 POC-GP/HA composites favored hMSCs differentiation in vitro

To evaluate the potential of both POC-GP materials for orthopedic application, the cytocompatibility of the new materials with different ratio of GP salts was first assessed by culturing hMSCs on the crosslinked polymer films for 24 h before the cell viability was tested by CCK-8. Polycaprolactone (PCL) films and Blank group without polymer films were used as controls. As shown in **Figure** 0.2, it was obvious that POC-GPCa films exhibited good cytocompatibility with less than 20% of viability reduction compared with the Blank control, which is comparable with that of commercial PCL films, but better than that of POC-βGPNa. In all three POC-βGPNa formulations, by increasing of the feeding

ratio of βGPNa to citric acid from 0.2 to 0.5, there was a significant decrease in cell viability, indicating that POC-0.2βGPNa and POC-0.3βGPNa might be the better candidate for tissue engineering application. Proliferation of hMSCs on different polymer films was also tested by using CCK8, which showed that all POC-βGPNa polymer films supported cell proliferation at least to a similar extent of PCL control films. Notably, POC-0.3GPCa films elicited a comparable proliferation rate of hMSCs to that in the blank control group, better than that on the PCL films. The above results together demonstrated the acceptable cytocompatibility of POC-βGPNa and the excellent cytocompatibility of POC-GPCa, even better than commercial PCL. POC-0.2βGPNa and POC-0.3GPCa were selected and named as POC-βGPNa and POC-GPCa, respectively, for the following stem cell differentiation and *in vivo* studies.

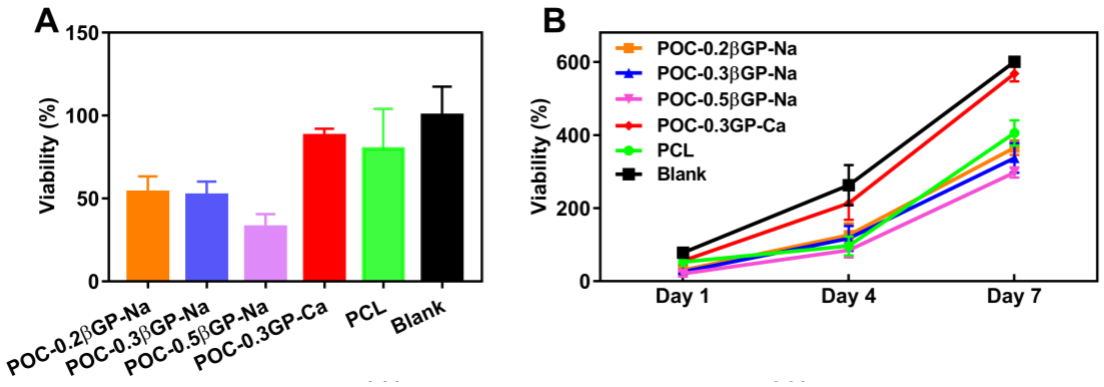

Figure 0.2 Cytocompatibility test of POC-GP films. (**A**) Cytotoxicity evaluation of hMSCs cultured on different polymer films at 24 h. (**B**) Proliferation of hMSCs on different polymer films for 1,4 and 7 days.

Given soluble citrate monomer at 200 μM supplemented in established osteogenic medium has been found to be the optimal concentration to promote osteogenesis progression [18], and β-GPNa in its solute form (from 2 mM to 10 mM) is already included

in the osteogenic medium. Also, the effect of GPCa, a food supplement for calcium and phosphate, on osteo-differentiation of stem cells is less focused on, probably because The solubility GP-Ca at pH 7.5 is around 5.7 mg/mL [67], which is much lower than that of βGP-Na (100 mg/mL). Therefore, in order to identify the effect of citrate, GPNa and GPCa on hMSCs differentiation separately, we prepared reductive osteogenic medium including only dexamethasone and ascorbate-2-phosphate and then supplemented citrate, GPNa and GPCa at 200 μM to culture with hMSCs. As shown in **Figure** 0.3, after 14 days of differentiation, the ALP expression in either βGPNa, GPCa, or citrate group was significantly higher than that in control group on day 7 and 14, while on day 21 no difference in ALP level between all groups was found, suggesting their comparable osteopromotive effect mainly at the early-to-middle stage of differentiation.

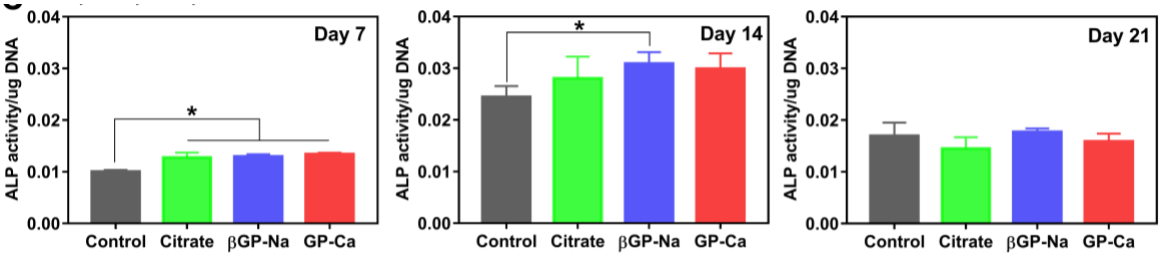

Figure 0.3 Effect of two GP salts, βGPNa and GPCa, and citrate at concentrations of 200 μM on hMSCs osteogenic differentiation on day 7, day 14 and day 21, evaluated by ALP expression.

To mimic the natural bone composition, POC-βGPNa and POC-GPCa pre-polymers composited with 60% HA by weight, which were then fabricated into flat disks before crosslinking. POC/60%HA and PLGA/35%HA composite disks were also prepared in the same way as controls. To evaluate the potential of POC-GP/HA composites in orthopedic applications, hMSCs were differentiated on different composites in osteogenic

medium and the production of alkaline phosphatase (ALP) was tested after 7, 14, and 21 days. A significant increase in ALP expression was observed on POC-GPCa/HA at all three time points tested, as compared to all other groups (**Figure** 0.4 **A**). In comparison, the incorporation of POC-βGPNa seemed not to further promote osteogenic differentiation, shown as similar ALP production level of stem cells cultured on POC-βGPNa/HA to that on POC/HA. Also, as expected, all citrate-based composites supported the enhanced osteogenic differentiation, as compared to the PLGA/HA composites, especially on day 14 and 21, consistent with our previous studies showing the osteopromotive capability of citrate-based composites [18, 68].

Real-time PCR revealed a marked increase in all three osteogenic markers (including Runx2, Collagen type I and osteopontin) when culturing on POC-GPCa/HA in established osteogenic medium, compared with that on POC-βGPNa/HA. It indicated that POC-GPCa/HA, possessing better cytocompatibility, also provided better support for osteogenic differentiation progression and bone related extracellular matrix production (collagen type I and osteopontin), confirming a superior osteopromotive effect of POC-GPCa/HA over POC-βGPNa/HA. Meanwhile, the extracellular matrix production and calcium deposits that produced by hMSCs cultured for 14 days were observed by SEM. As shown in **Figure** 0.5, when cultured in established osteogenic medium, the formation of fibrous extracellular matrix was evident in all three material groups with more calcium deposits formed in both POC-GP groups. When cultured in growth medium, cells tended to display normal stem cell morphology with smooth cell surface, except in the POC-GPCa/HA, signs of a few fibrous extracellular matrix were evident. Small amount of calcium deposits was also observed in both POC-GP/HA groups. Taken together, the above

results revealed that although soluble βGPNa and GPCa possess comparable osteopromotive effect, and the prepared POC-βGPNa/HA and POC-GPCa/HA composites both supported the *in vitro* formation of calcium deposits probably by releasing βGPNa and GPCa as organic donor, POC-GPCa/HA composites, in comparison with POC-βGPNa/HA, were more supportive for intracellular osteo-differentiation molecular progression and the production of bone-related extracellular matrix, probably due to its excellent cytocompatibility and its faster degradation rate to release osteopromotive citrate and GPCa. Considering organic phosphate availability and the cell produced ECM network (serving as biomineralization template) both are critical for cell-mediated controllable biomineralization, POC-GPCa/HA composites might be a superior candidate for orthopedic application.

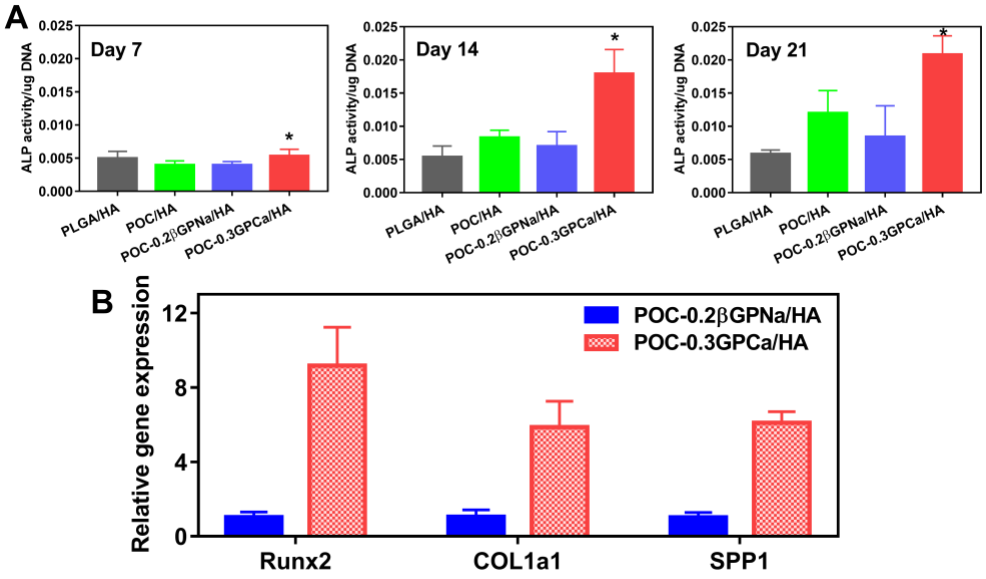

Figure 0.4 Osteogenic differentiation on hMSCs on composites. (**A**) ALP production of hMSCs differentiation on the POC/HA, POC-βGPNa/HA and POC-GPCa/HA composite disks in osteogenic medium for 7, 14, and 21 days, compared with that on PLGA/HA (*

indicating P<0.05). (**B**) Gene expression of *Runx-2*, *Col1a1*, and *SPP1* in differentiating hMSCs cultured on polymer composites for 14 days, as analyzed by real-time PCR (* indicating P<0.05).

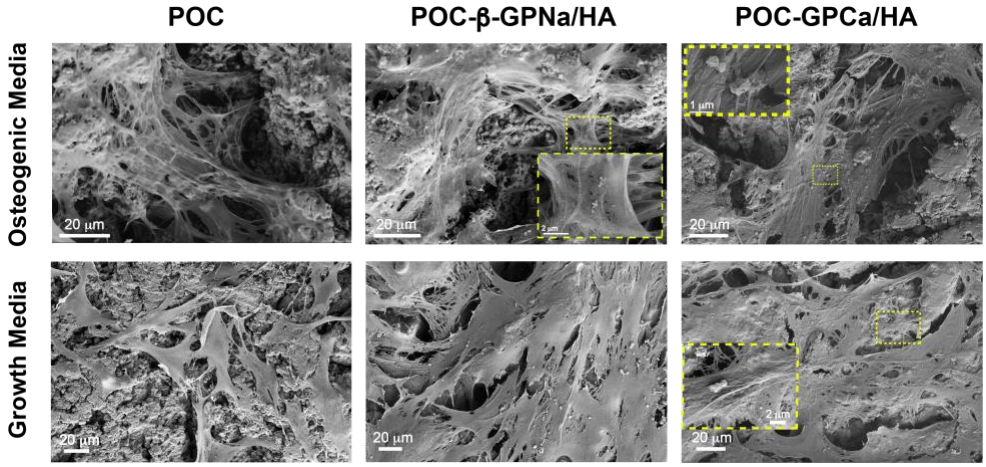

Figure 0.5 Mineral deposits and ECM formation of hMSCs on POC/HA, POC-βGPNa/HA and POC-GPCa/HA composites with or without osteogenic inducers under SEM.

3.3.3 POC-GP/HA composite microparticles supported hMSCs differentiation in vitro

To further translate the new POC-GP for orthopedic applications, we fabricated the POC-βGPNa/HA and POC-GPCa/HA composites into microparticulate scaffolds by preparing crosslinked porous polymer/60%HA composite scaffolds through salt leaching (pore size: 250-425 μm), followed by grinding and sieving. Microparticles at different size ranges (<150 μm; 150-250 μm; 250-425 μm; >425 μm) were obtained and POC/HA microparticles were also prepared in the same way as control. The surface feature of three different kinds of microparticles at different sizes were observed by using Scanning

Electron Microscope (SEM; **Figure** 0.6 **A**), which showed a more evident "ridge" surface feature on microparticles with larger particles size (>250 μm), while with a rougher surface on microparticles with smaller particle size (<150 μm), probably due to the exposure of bioactive HA through grinding. Next, in order to explore the effect of particle size on osteogenic differentiation, we differentiated hMSCs on both POC-βGPNa/HA and POC-GPCa/HA microparticles at different size ranges. The ALP production of hMSCs revealed a similar trend for both POC-βGPNa/HA and POC-GPCa/HA microparticles (**Figure** 0.6 **B**), that is, microparticles with the size of <150 μm promoted the osteo-differentiation at early time point (day 7), probably because of the more exposed bioactive HA; while larger size of microparticles were shown to favor ALP production when the differentiation proceeded to middle stages (day 14), probably due to the rough surface feature facilitating cell adhesion and 3D interaction for differentiation [18]. Eventually, at late stage (day 21), hMSCs cultured on microparticles with different sizes all produced ALP to a similar extent. Therefore, a mixture of microparticles of different sizes were used in the following *in vivo* evaluation of their capability to support bone regeneration.

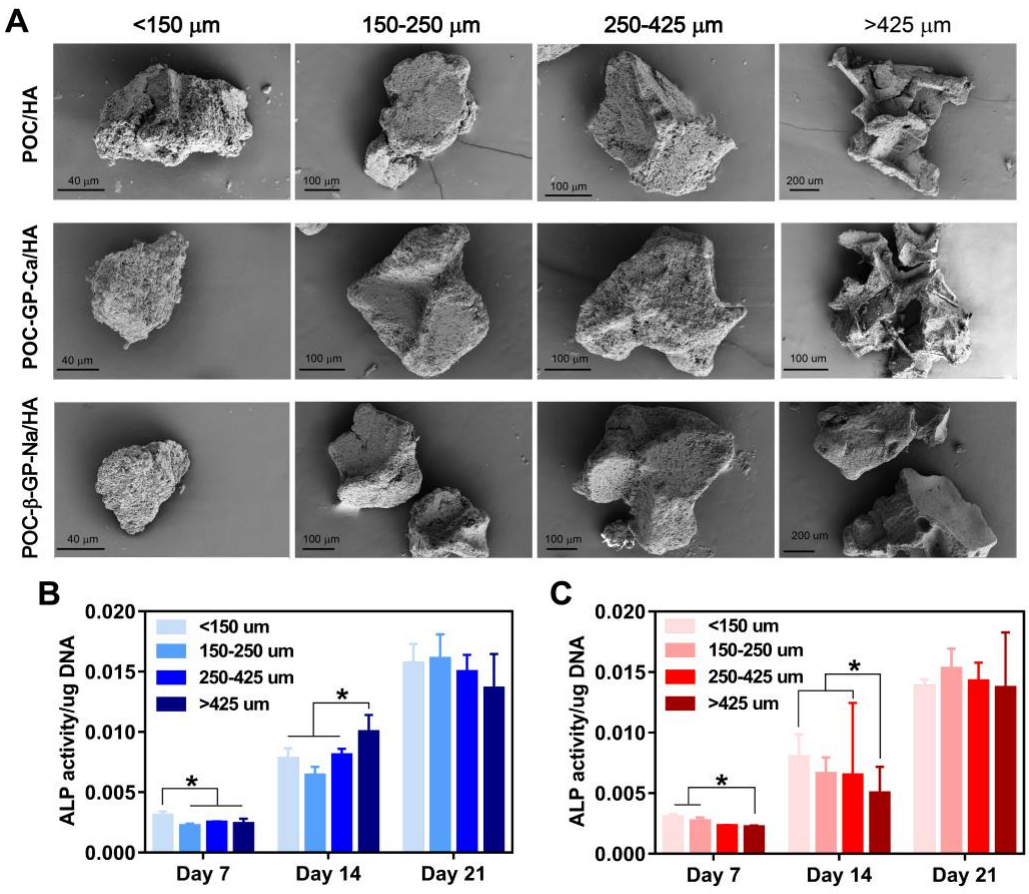

Figure 0.6 Composite microparticles and the effect of microparticle size on osteogenic differentiation. (**A**) SEM images of the composite microparticles at different size range (<150 µm; 150-250 µm; 250-425 µm; >425 µm). (**B**) ALP production of hMSCs differentiation in reductive osteogenic medium on POC-βGPNa/HA and (**C**) POC-GPCa/HA composite microparticles at different size ranges for 7, 14, and 21 days (* indicating $P<0.05$).

3.3.4 POC-GP/HA microparticles promoted bone regeneration in femoral condyle defects

Based on the results from *in vitro* studies, we further investigated the *in vivo* osteopromotion functionality of both POC-βGPNa/HA and POC-GPCa/HA microparticle scaffolds in rabbit femoral condyle defect, the standardized and reproducible defect model without the need for fixation, that been successfully applied to evaluate the efficacy of particulate bone grafts in bone repair [18, 69]. POC/HA microparticles were also implanted as materials control, while defects without any implants served as negative control. At 4, 8 and 12 weeks after implantation, microCT analysis was performed to evaluate the new bone formation within defects. The 3D reconstructed images (**Figure 0.7 A**) of the defects clearly showed the new bone ingrowth in all three scaffold groups occurring from the defect edge towards the defect center resulted in gradually decrease of defect size. The bone ingrowth speed in all three scaffold groups was much higher than that in the control group without any microparticles implanted, although new bone ingrowth was also observed in the control group from 4-12 weeks. It is also supported by the 3D reconstructed images of new bone formation within defects images (**Figure 0.7 B**), displaying significantly less density signal in the Control group than that in the three materials groups at each time point. Moreover, both **Figure 0.7 A & B** showed an enhanced new bone formation in the POC-GPCa/HA group, as compared with that in POC-βGPNa/HA and POC/HA group, in accordance to ALP activity tests on polymer/HA composites (**Figure** 0.4 **A**). Compared with CBPB/HA, iCMBA/HA and BPLP-PSer, which were citrate-based polymer/HA composites developed in Yang lab, POC-GPCa/HA showed excellent osteointegration ability and reached a complete new born ingrowth surrounding implants

in a relatively short time (8 weeks) [18, 58-59]. Quantitative micro-CT analysis data (**Figure 0.7 C**) further confirmed that a significantly higher BV/TV value in the POC-GPCa/HA group as compared to other control groups, especially at 12 weeks. These *in vivo* results supported the superior performance of POC-GPCa/HA microparticles in promoting new bone formation, which is consistent with the *in vitro* differentiation results (**Figure 0.7**).

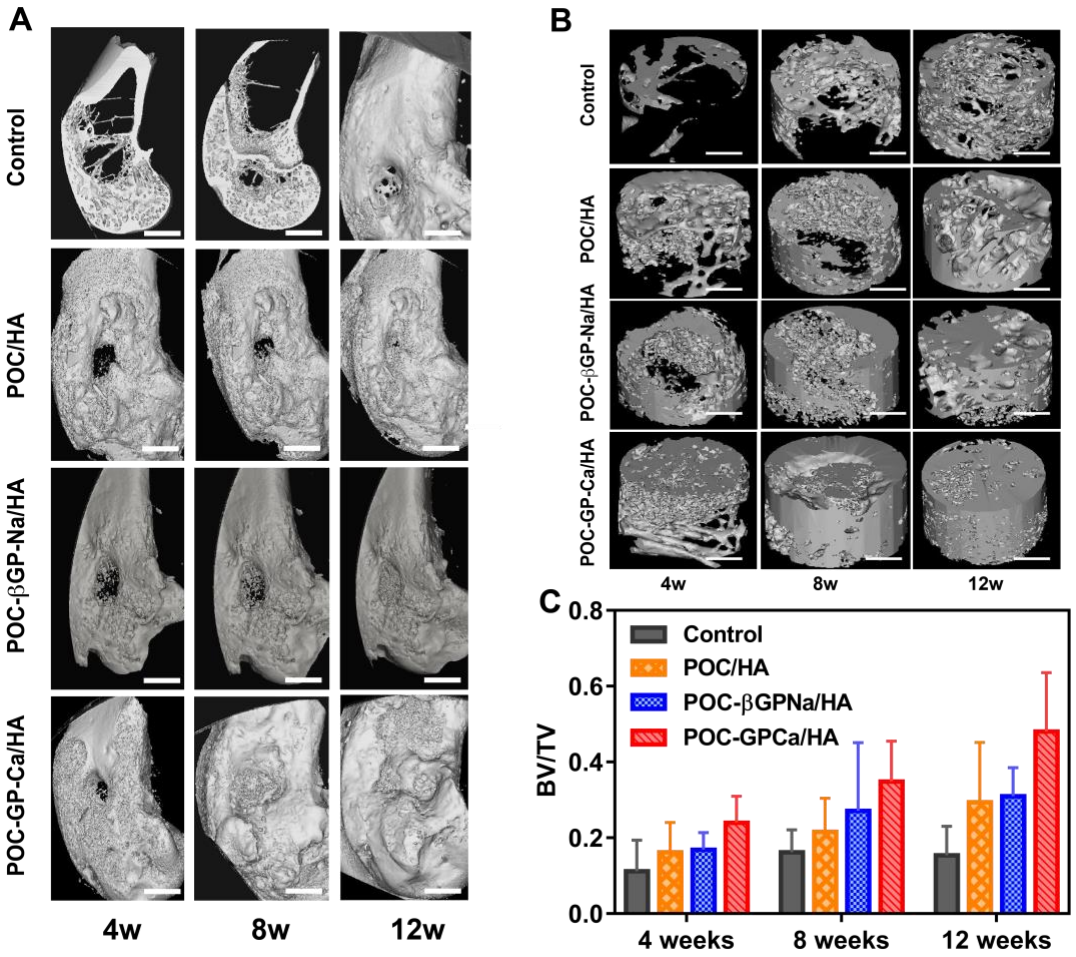

Figure 0.7 Micro-CT evaluation of new bone formation. (**A**) 3D reconstructed micro-CT images of the femoral condyle defects at 1, 2, and 3 months after implantation. Scale bar: 5 mm. (**B**) 3D reconstructed micro-CT images of the new bone formation within the defects at 1, 2, and 3 months after implantation. Scale bar: 1 mm. (**C**) Quantitative micro-CT analysis of the BV/TV value to evaluate new bone formation.

Histological analysis of the newly formed tissue within the defects were further performed. In the representative Masson staining images of three different microparticles at 1 month of implantation (**Figure** 0.8), blue-stained immature bone growing from the defect edge towards its center through the microparticle scaffolds, with intimate interaction between new bone and materials while with fibrous connective tissue filled in the defect center, can be evidently observed in all material groups. There is no separation, such as fibrous capsule between the implants and host bone tissue, demonstrating the excellent osteoconductivity and osteointegration of all citrate-based composite microparticles. At 8-week post implantation, more blue-stained bone was found to deposit directly onto the microparticles, while the red-stained mature bone started to be visible around the POC-GPCa/HA implants, suggesting that the POC-GPCa/HA might favor the bone maturation compared with other control groups.

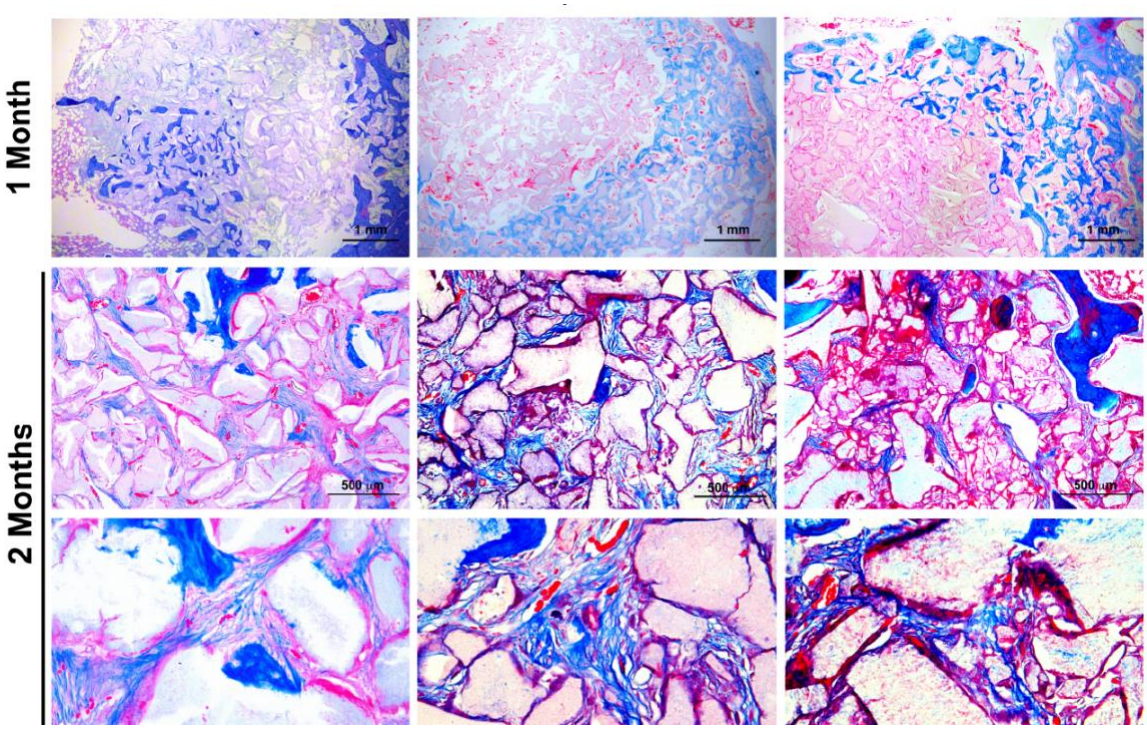

Figure 0.8 Masson staining images of the newly formed bone within the defects implanted with POC/HA, POC-βGPNa/HA and POC-GPCa/HA at (**A**) 1 month and (**B**) 2 months after implantation.

H&E staining images at 1 month (**Figure 0.9 A, B**) further confirmed a close contact between the new bone and both POC-βGPNa/HA and POC-GPCa/HA microparticles. The connective tissue in POC-GPCa/HA group (**Figure 0.9 D**) that intertwined with microparticles in the defect center and close to the bone growth front seemed to be firmer than that in the POC-βGPNa/HA group even after 8 weeks (**Figure 0.9 C**). Direct bone deposition with bone-making osteoblasts lined up around the microparticles and with visible trapped osteocytes were observed in the POC-GPCa/HA group at 4 weeks. Together with the micro-CT analysis, these results consistently suggested

that POC-GPCa/HA microparticles possessed excellent osteoconductivity and promoted bone regeneration in the femoral condyle defects, serving as a better candidate than POC-βGPNa/HA for orthopedic applications.

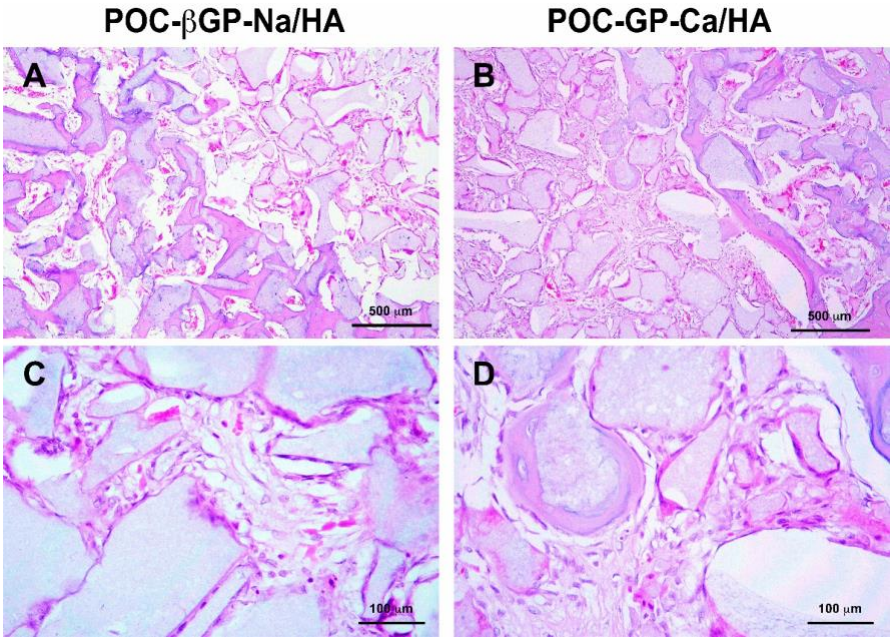

Figure 0.9 H&E staining images of tissues surrounding microparticle implants. (**A**) POC-βGP-Na/HA at 1 month; and (**B**) POC-GP-Ca/HA at 1 month (scale bar = 500 μm). (**C**) POC-βGP-Na/HA at 2 months and (**D**) POC-GP-Ca/HA at 1 month (scale bar = 100 μm)

3.4 Conclusions

In conclusion, in the present study we developed a new class of osteopromotive bioactive biodegradable materials, POC-βGPNa and POC-GPCa with widely tunable mechanical properties and degradation. POC-GPs could be synthesized by a simple and cost-effective polycondensation method. Within the formulation investigated, POC-GPCa/HA composite demonstrated better bioactivity in promoting osteopromotive differentiation of hMSCs *in vitro* and further improving bone regeneration in rabbit femoral condyle defects. The development of POC-GP expands the repertoire of the well-recognized citrate-based biomaterials to meet the ever-increasing needs for functional biomaterials in tissue engineering and other biomedical applications.

4 Chapter

Renewable and Degradable Citrate-based Resins and Filtration Devices for Purification of Liquids

4.1 Introduction

Immobilized chelating agents promise a revolution in deodorization of oils, maintaining the chelating capability of soluble metal chelates while eliminating the consequences of contamination of the finished product with said agents. Additionally, utilization of chelants eliminates the necessity of hot water addition, which increases the purification time and cost (via required water removal). Immobilized CBR polymers also promise to increase thermal stability over raw citric acid, removing this limitation from the heat bleaching process. Thus, CBR filtration columns have the potential to achieve one - step filtration and deodorization. Citrate based polymers are inexpensive, easily synthesized, relatively low toxicity (many being designed as implantable biomaterials for tissue engineering), and fully degradable via hydrolysis when exposed to water [70]. Citric-based polymers preserve the surface pendent carboxyl groups of citric acid, which are responsible for metal chelation [71]. Inspired by column filters for water treatment and filtration of laboratory chemicals, as well as early column-based systems for vegetable oil purification [72], deodorization and metal ion filtration are achieved through the use of CBR porous structures as the stationary phase, absorbing metal ions through surface contact with oil while allowing oil heating to maintain sterilization and heat bleaching. CBR disks are fabricated as individual units, capable of being stacked within the column sleeve, leading to an easily expandable and replaceable system capable of increasing oil retention time and

ion absorption during each filtration cycle. The mechanical properties and durability of citrate-based polymers as well as the highly porous nature of designed CBR disks lead to a column capable of enduring high pressure and velocity fluid flow while maximizing fluid surface contact. Additionally, once saturated with metal ions, CBR columns can be renewed via a simple washing process utilizing ethylenediaminetetraacetic acid (EDTA) via ion exchange due to the stronger chelating ability of EDTA compared to citric acid.

The deodorization process of crude oil and other similar fluids not only removes unpalatable flavors, but also has a crucial impact on refined liquid quality, including the stripping of volatile contaminants and degradation of undesirable color pigments. Deodorization is typically achieved via heat bleaching, in which a stripping agent is passed through a hot oil stream at low pressure for an extended time period in order to remove volatile compounds. Complete sterilization is simultaneously achieved due to the bactericidal bleaching temperature. Chelates, commonly citric acid, are added during deodorization to remove residual metals, such as copper, iron, calcium, and magnesium, and to increase stability during storage.

Despite improvements in deodorization technology, the principles and materials for deodorization have remained relatively unchanged, with significant potential for further increases in both efficiency and effectiveness of the process. Current purification methods require the addition of hot water to the raw oil in order to achieve chelant solubility; however, not only does this necessitate the addition of water that must be subsequently removed from the oil to minimize moisture content, but the elevated temperature decomposes the citric acid (decomposition beginning at 104°C under the typically utilized reduced pressure of deodorization). Phosphoric acid, as an alternative chelating agent,

offers better feasibility, purity and antioxidative effects in the liquid state, but is limited by higher costs and undesirable phosphate waste product buildup in streams and other water supplies.

Thus, economical, readily expandable, and reusable CBR filtration columns were fabricated capable of simultaneous heat bleaching, sterilization, and metal filtration while maintaining the purity of the final product. The method we used is universal and readily scalable. Through this method, 1) resins may be modified to achieve different mechanical properties and degradation profiles by different formulations and reaction conditions, 2) a wide variety of filter morphologies (.i.e. thickness, shape, porosity, inclusion of channels, surface roughness, etc.) may readily be achieved to tailor to specific filtration devices or requirements, 3) resin surfaces may be modified with different chelating molecules, such as polyethyleneimine, to improve the purification efficiency, 4) polyphenol derivative based coatings may be applied to harness the resin with antibacterial and antifouling properties. Fabricated columns are composed of low-cost materials which are degradable and disposable with minimal environmental impact, leading to a green and cost-effective filtration unit for oil, wastewater, and body fluid purification.

4.2 Materials and methods

4.2.1 Materials

1,8-octanediol (98%) and citric acid (99.5%) were purchased from Alfa Aesar. All remaining chemicals were purchased from Sigma-Aldrich (St Louis, MO) and used as received unless stated otherwise.

4.2.2 CBR prepolymer synthesis

CBR pre-polymer was synthesized by bulk polymerization using citric acid and polyols in 1.0:1.1 feeding ratio. Briefly, monomers were stirred mechanically and melted under nitrogen protection at 160°C in a silicon oil bath. Then the temperature of the system was lowered to 140°C, followed by stirring for 1-2 h to create the pre-polymer. The reaction was quenched by 1,4-dioxane and purified in deionized water followed by lyophilization. The purified pre-polymer was dissolved in 1,4-dioxane (30 wt/wt%) for future use.

Citrate-based resins were synthesized via a convenient, one pot polycondensation reaction similar to previous citrate-based polymers [70]. CBRs are further thermally crosslinked to fabricate CBR films or mixed with salt or other porogens followed by thermal crosslinking and porogen leaching to fabricate porous CBR scaffolds.

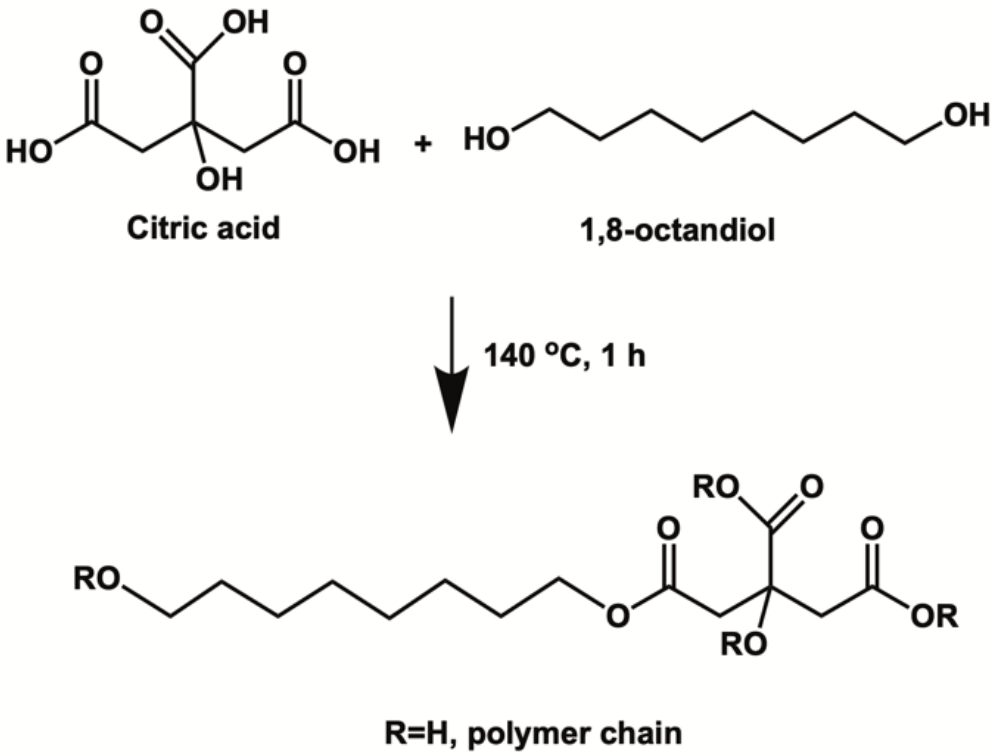

Figure 0.1 Synthesis and Characterization of POC polymers.

4.2.3 CBR fabrication

Porous CBR scaffolds were fabricated by mixing 30% prepolymer solution with NaCl salt particles (>425 um, 250-425 um) with different ratios into slurry. The slurry was cast into a Teflon dish, followed by thermal crosslinking at 80°C for 3 days. Porous crosslinked CBRs were achieved by leaching salt in water with subsequent freeze drying.

To prepare polymer films, pre-polymer solution was cast in Teflon dishes and the solvent was allowed to evaporate. The dried pre-polymer was then thermally crosslinked to obtain a crosslinked polymer film.

A 15 mm diameter circular punch was used to make scaffold discs. These disks were then crosslinked at the desired crosslinking conditions (80 °C - 120 °C, with or without vacuum, 1-3 days).

4.2.4 CBR morphology observation

To observe morphology of porous scaffolds, field emission scanning electron microscopy (FESEM, Zeiss) was used to capture and analyze images at 5 kV. Before FESEM observation, the scaffold was fractured in liquid nitrogen and coated with 5 nm iridium using sputter coater (Leica) before imaging.

4.2.5 Mechanical tests of CBR scaffolds

Tensile tests of polymer films were conducted on an Instron 5966 machine equipped with a 500 N load cell. Samples were cut into rectangular strips and pulled until failure at a

speed of 500 mm min^{-1} to obtain stress–strain curves. The initial slope (0–10%) of the stress–strain curve was used to determine the initial modulus of each sample. Six specimens were averaged for each sample, and the results were presented as (means ± standard deviation).

Compressive strength testing was carried out with an Instron 5966 machine equipped with a 500 N load cell. Scaffolds were cut into cylinder shapes and pressed until 50% displacement at a speed of 50 mm min^{-1} to obtain stress–strain curves. The initial slope (0–10%) of the stress–strain curve was used to determine the initial modulus of each sample. Six specimens were averaged for each sample, and the results were presented as means ± standard deviation.

4.2.6 Degradation, leaching and swelling properties of CBR scaffolds

Degradation properties were studied *in vitro* with polymer film samples placed in tubes containing 10 mL of NaOH solution (0.05 M) or phosphate buffered saline (PBS, pH=7.4) and incubated at 37°C. Samples were weighed before degradation to find the initial mass (W_0). At each determined time point, samples were washed thoroughly with deionized water 3 times. After lyophilization, samples were weighed to measure the remaining mass (W_t). Six parallel specimens were averaged for each sample, and the results were presented as means ± standard deviation. The percent mass loss was calculated based on the following equation:

$$Mass\ loss\ (\%) = \frac{W_0 - W_t}{W_0} \times 100 \qquad Equation\ (2)$$

To evaluate the swelling ratio and leaching products of CBRs in oil and aqueous phase, porous disk-shape CBRs were weighed (W_0) and submerged into soybean oil or DI water for up to 7 days. At each determined time point, the excessive oil or water on scaffolds were slightly dried by Kimwipe and the swollen networks was weighed. Then samples were washed thoroughly with deionized water or hexane for 3 times and freeze dried. Six parallel specimens were averaged for each sample, and the results were presented as means ± standard deviation.

The swelling ratio and solid content percentage were calculated based on the following equations:

$$Swelling\ ratio\ (\%) = \frac{W_s - W_d}{W_d} \times 100 \qquad Equation\ (1)$$

$$Leachables\ (\%) = \frac{W_0 - W_d}{W_0} \times 100 \qquad Equation\ (2)$$

Here, W_0 represents the initial dry weight of CBR scaffolds, W_s represents the network weight after the leaching or swelling in water or oil, and W_d represents sample remaining mass after washing and lyophilization.

4.2.7 Design of filtration loop system

The filtration loop was assembled with an oil transfer pump (Macro-UP3/OIL, UP6/OIL, James town distributors), customized filter holder (steel, made in PSU machine shop), food grade tubing, and an oil reservoir (**Figure** 0.3)

CBR filtration columns were constructed by stacking multiple disk shaped CBR scaffolds vertically within a cylindrical, glass containment tube with an inner diameter equivalent to the diameter of the CBR disks. Soybean oil was filtered through the column and aliquots were removed at various time points to compare ion concentration to initial concentrations.

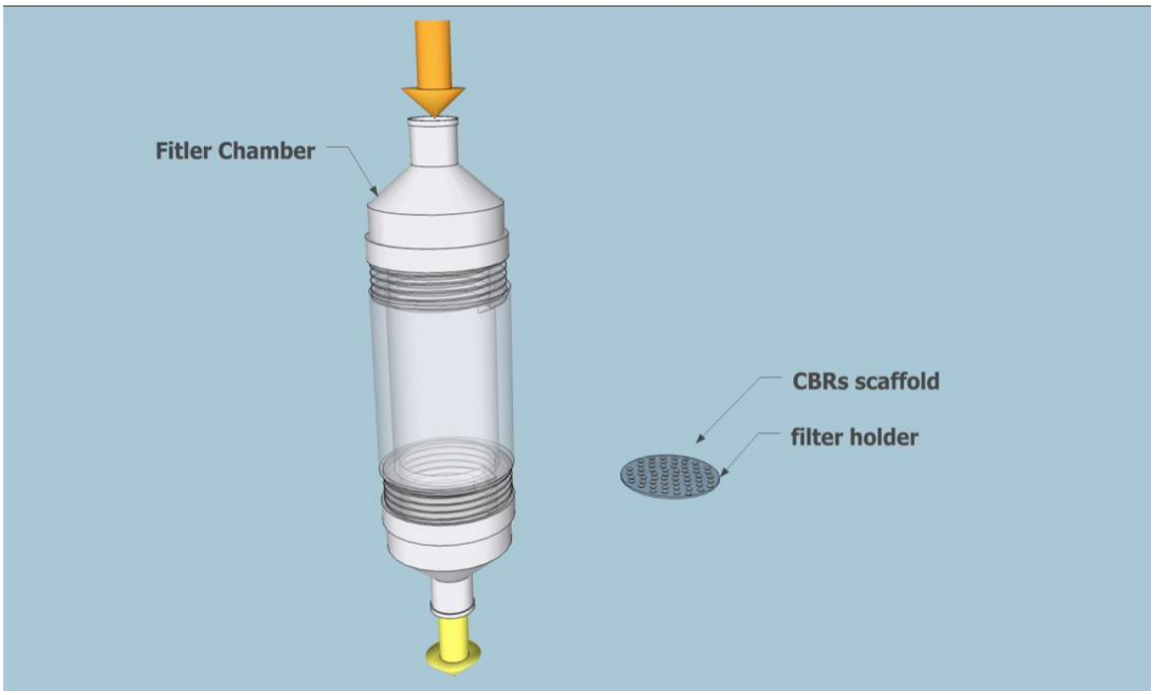

Figure 0.2 Schematic demonstration of the design of the filter chamber filled with citrate-based resins.

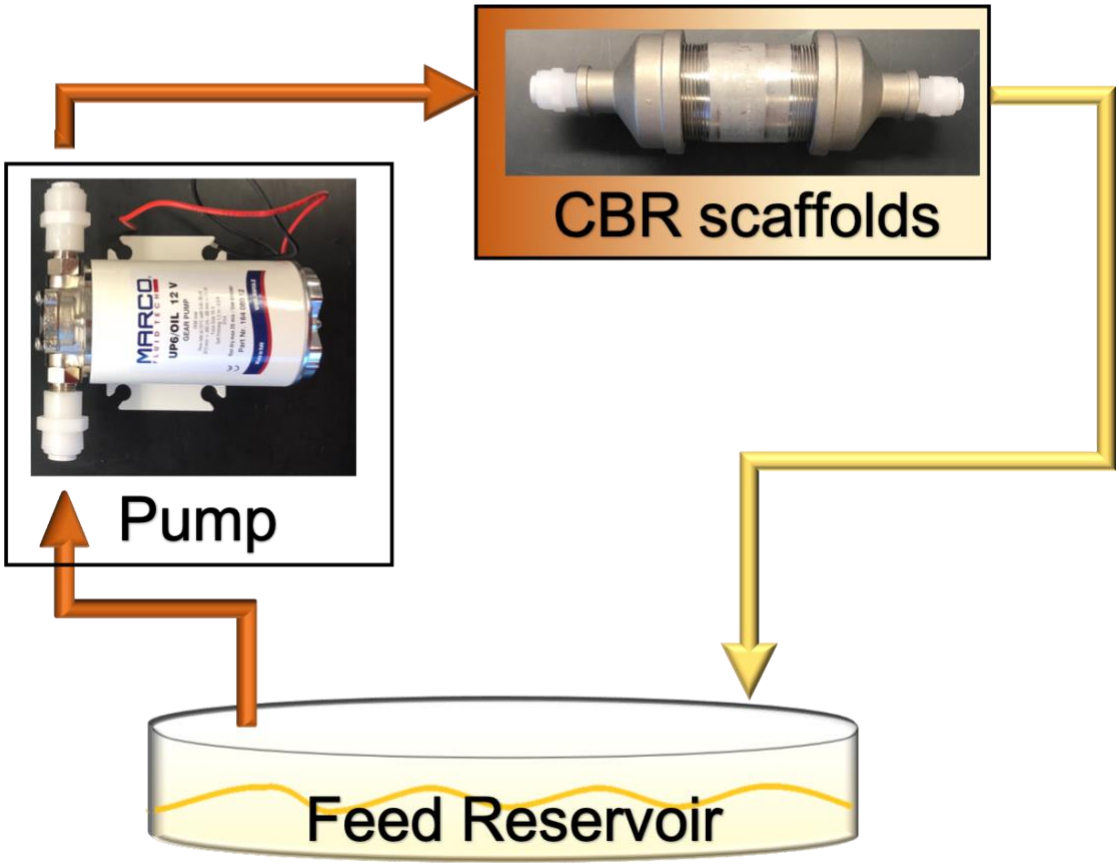

Figure 0.3 Schematic demonstration of the overall design of the filtration loop system composed of a filter chamber and a pump.

4.2.8 Metal removal of vegetable oil by CBR scaffolds

Spiked vegetable oil was made by addition of organic metal standard oil solution at different concentrations. The CBR filters were weighed before and after filtration. Once CBRs were installed into the chamber and spiked oil was added into the oil reservoir, the pump was turned on for different time periods. Small amounts of oil were taken out of the reservoir for future characterization. The filtration loop was rinsed with SBO 3 times before each use.

4.2.9 ICP-AES

ICP-AES were used to determine trace metal content before and after each time filtration [73]. After acid digestion, the metal ion aqueous solutions were injected into or ICP-OES to determine ion concentration. The ultimate metal concentration in oil was calculated based on the dilution factor. Calibration was done for instrument and specific metals before running samples.

The metal chelating ability of CBR scaffolds will be assessed by immersing samples into water or vegetable oil-based solutions containing known initial concentrations of metal ions. Following incubation for various time, fluid will be removed and the remaining ion concentrations will be quantified using HPLC with reference standards. Ion binding/ gram polymer will be determined by comparing the initial and final ion concentrations of the fluid. The effect of incubation time and ion concentration on ion removal will be determined. Common ions including sodium, potassium, magnesium, zinc, iron, aluminum and titanium will be tested to verify the versatility of the filtration system. Combinations of multiple ions will also be tested to determine the effect of competing ion species on chelation ability. The ability to remove ions from and renew CBR resins will be determined by incubating ion saturated samples in EDTA solution and testing the ability of EDTA to fully remove ions from the resin scaffolds.

CBR scaffolds are able to chelate a significant quantity of ions regardless of ion species and initial ion concentration. Ion chelation could be increased by increasing incubation time, by decreasing crosslinking time (to preserve more chelating side groups) or by increasing PEI or citric acid content. Additional chelating pendant groups could also be added if necessary, via polycondensation or other chemical modification procedures.

$$Removal\ effiency\ (\%) = \frac{C_f - C_p}{C_f} \times 100 \qquad Equation\ (3)$$

Where Cp and Cf (ppm) are the heavy metal concentration in the filtrate and feeding oil, respectively.

4.3 Results and discussion

4.3.1 Structural characteristics of citrate-based resin membranes

The present research relates to degradable polymeric resins for fluid purification, more particularly, this relates to the method of preparing degradable polymeric resin through a facile one-pot reaction and design of the purification system and their applications in liquid purification. The basic chemistry utilized here is polycondensation between hydroxyl and carboxylic acid groups or intermolecular crosslinking between resin molecules. Polyester can be synthesized under mild conditions and broken-down during degradation under similarly mild conditions.

The surface morphologies of the CBR were characterized by FE-SEM, as shown in **Figure** 0.4. The pore sizes in CBR were regulated by salt particles in different sizes, ranging between 150–425 μm. From images in 500 X amplification (**Figure** 0.4 **B, D**), they displayed high degrees of pore interconnectivity to ensure fluid filtration and high porosities to maximize available surface area during purification. In the future, pore interconnectivity could be improved by adding poly (vinyl alcohol) to salt as a particle binder.

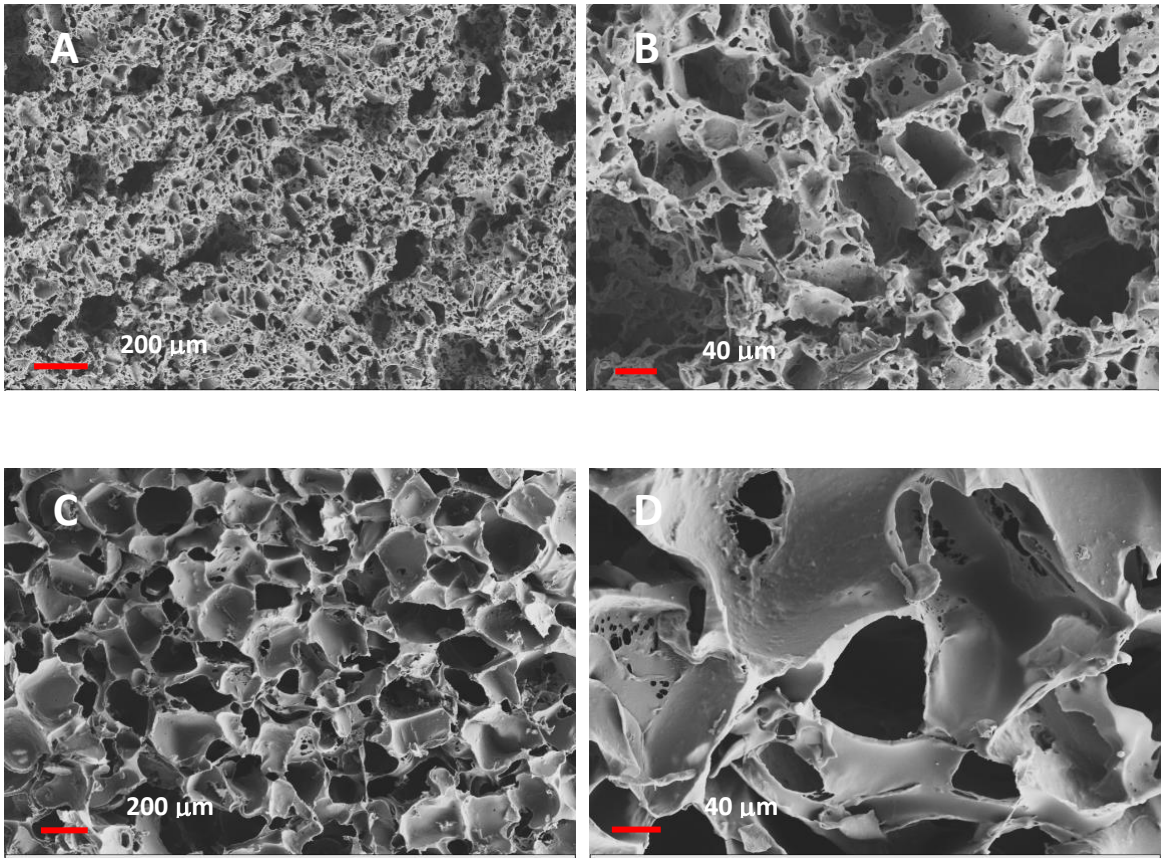

Figure 0.4 SEM images of porous structure of CBR scaffolds made with NaCl salt particles in different. Scaffolds are made with 250-425 μm NaCl particles with 80% porosity in 100 X (A), and 500 X (B) amplification and 150-250 μm NaCl particles with 80% porosity in 100 X (C), and 500 X (D) amplification.

In soybean oil filtration application, synthesized CBRs should remain thermally stable both at room and sufficient mechanical properties for handling and to withstand flow conditions (~300 kPa). **Figure** 0.5 showed the mechanical test data of pure CBR film acquired at room temperature, which represents a classic stress-strain curve of elastomer. The initial tensile modulus of CBR is 3.85 MPa and the tensile strength is 3.23 MPa. The mechanical properties can be further improved by changing crosslinking conditions, addition of functional monomer and processing methods. The mechanical tunability enable the

adaption of CBR in a larger scale operation in industry and various applications in other fields.

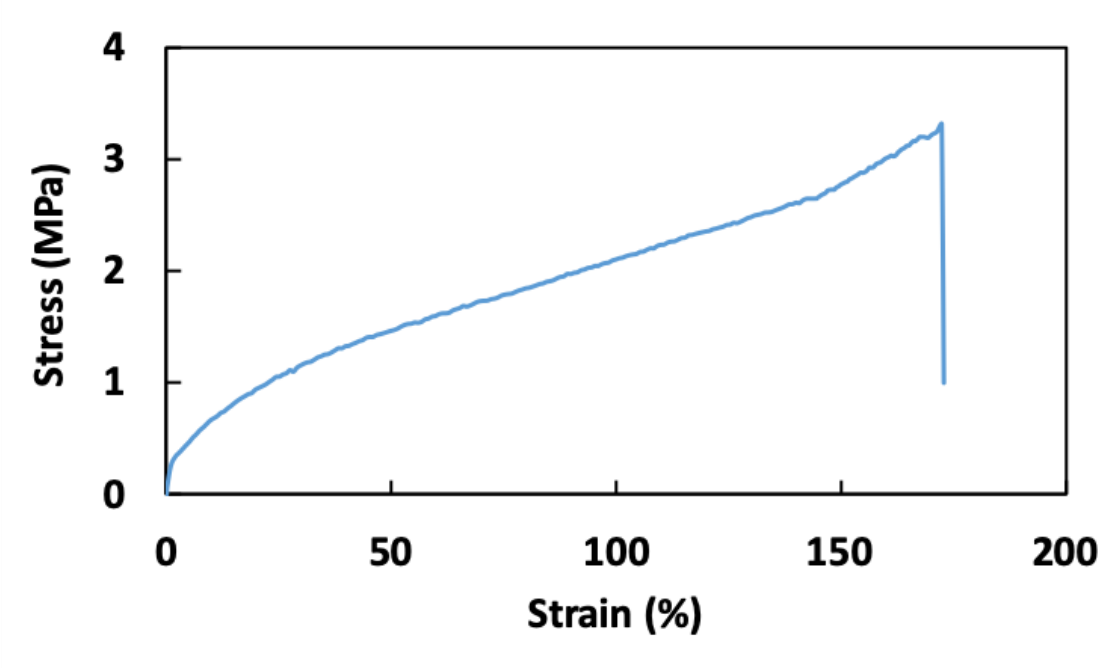

Figure 0.5 Stress-Strain curve to show the mechanical properties of CBRs

4.3.2 Degradation, swelling and leaching properties of CBR

In soybean oil filtration application, synthesized CBRs should display minimal leachable fraction and swelling to maintain shape integrity and minimize contamination of filtered fluids. The percentage of leaching products in oil and aqueous phase are shown in **Figure** 0.6. in water, CBRs leached 1.8% of the bulk scaffold on day 1 and it increased to 4.2% on day 7. In comparison, CBRs showed 1.1% leaching products on day 1 submerging in vegetable oil and it gradually increased to 1.7% on day 7. Meanwhile, CBRs showed a relatively low swelling ratio in oil ranging between 0.08% to 1.9% in oil and a higher ratio ranging between 7.7% to 10.9% in water (**Figure** 0.7).

Overall, the relatively low leaching products percentage and swelling ration from CBRs in both aqueous and oil phase assured the safe usage of CBRs in food processing and bioengineering applications.

In the future, swelling, sol content, and mechanical properties can be improved by increasing the crosslinking times of scaffolds, altering the monomer molar ratios, or by decreasing porosity. Additionally, soluble fractions could be pre-leached from the polymer before use.

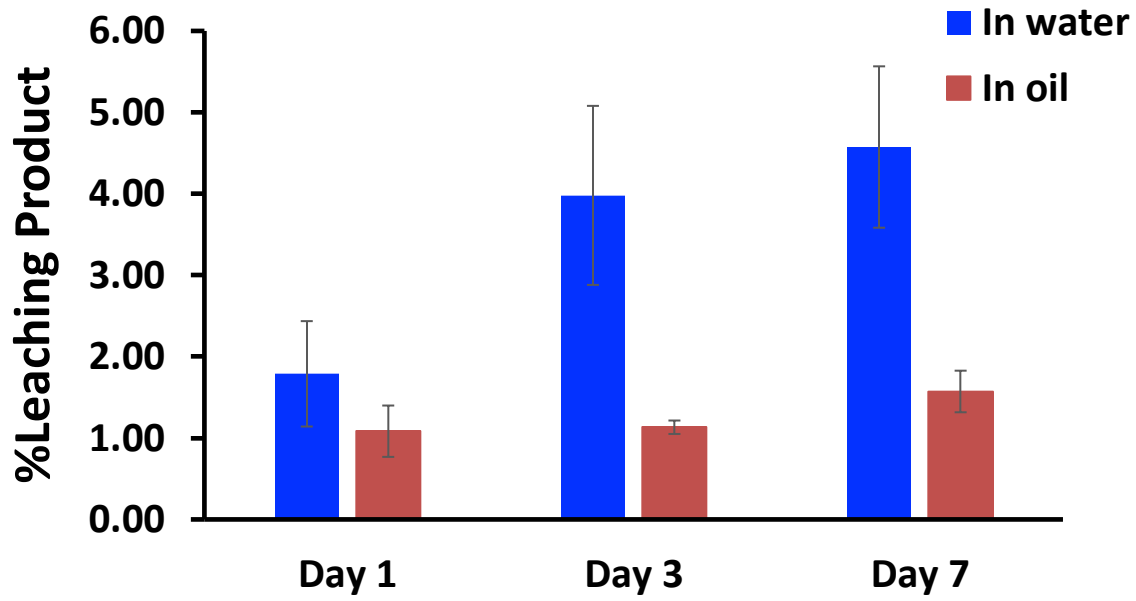

Figure 0.6 The percentage of leaching products of CBRs in oil and aqueous phase through 7 days.

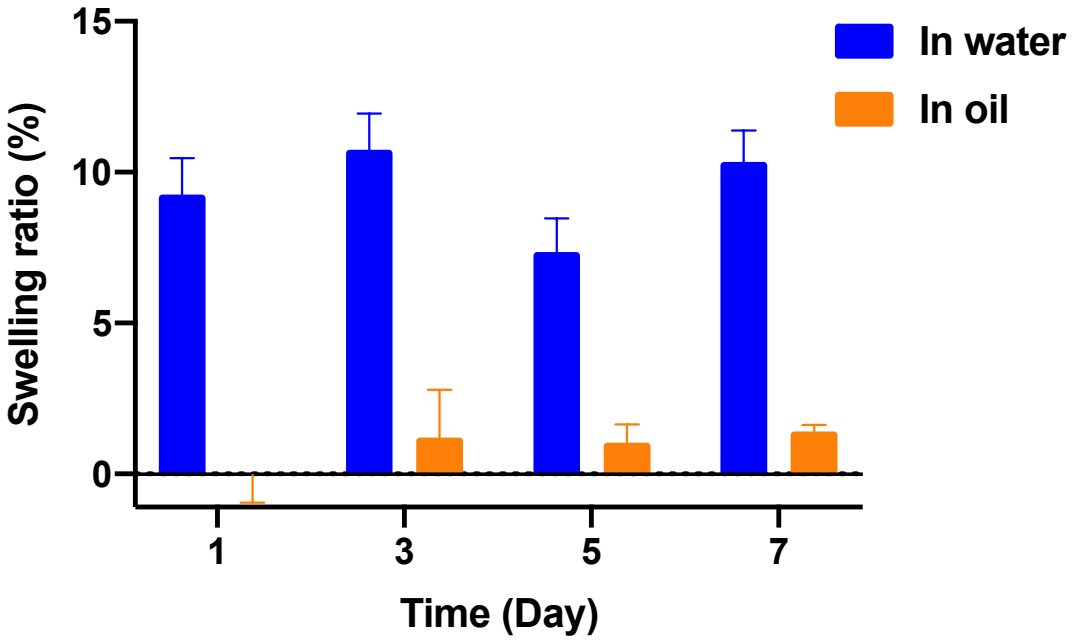

Figure 0.7 The swelling ratio of CBRs in oil and aqueous phase through 7 days.

4.3.3 Heavy metal removal efficiencies of different CBR membranes

Figure 0.8 showed the copper removal efficiency in oil filtration system by CBRs for 48 hours. The copper content decreased dramatically through the first 15 hours from 3.74 ppm to 0.14 ppm and it took another 33 hours to reduce copper concentration from 0.14 ppm to 0.08 ppm which is below the food standard [74].

The CBR membranes also showed recycling properties for reuse over multiple cycles in **Figure** 0.9. After running the copper-spiked oil for 24 hours, the CBR membranes were reused to purify another same amount of copper-spiked oil for other 24 hours, reducing the copper concentration from 3.74 ppm to 0.42 ppm.

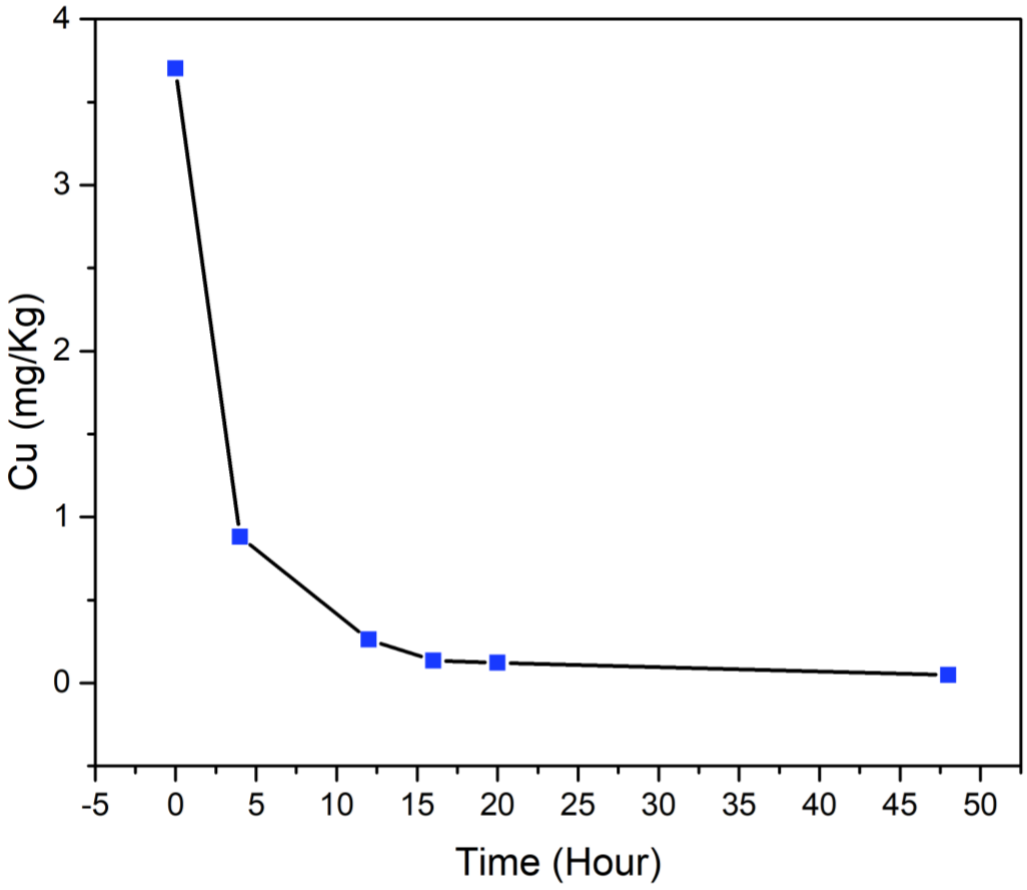

Figure 0.8 The copper removal efficiency in oil filtration system by CBRs for 48 hours.

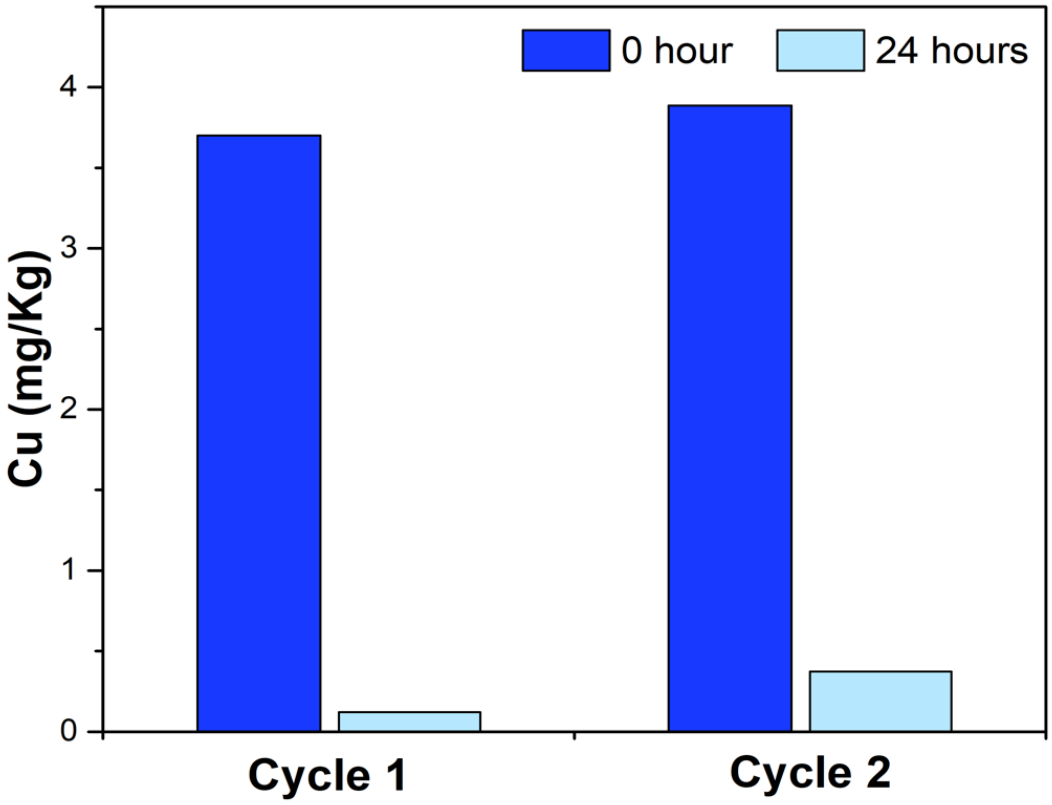

Figure 0.9 Demonstration of the copper removal efficiency in oil filtration system by CBRs in 2 recycles of 24 hours.

4.4 Conclusion

This work immobilized polymeric columns and make them readily modifiable for efficient deodorization and filtration. The above design of loop filtration system firstly proved the feasibility of using citrate-based resins to purify vegetable oils in lab or pilot studies, which holding great potential in transforming this application in food industry. Besides, the low leaching and swelling percentage ensured the stability, safety, and sustainability of CBR. Finally, the high removal efficiency of heavy metal and the recyclable properties showed solid evidence of the successful heavy metal purification of vegetable oil in the assist of

CBR chelating properties. On the other hand, due to the functional groups existing in CBR, future modification can be done by coating polyphenol derivatives, PEI or other functional molecules to harness the resin with antibacterial and antifouling properties to overcome potential microorganism contamination via a rapid one-step fabrication [75].

It is the first time to report that degradable and renewable citrate-based polyester was fabricated and used to purify oil. A renewable, non-toxic, one-step purification system, utilizing degradable, citrate-based resins (CBRs) as chelating agents was built based upon our previous research experience with citrate based polyester biomaterials. It is also demonstrated that the obtained polyester resins are capable of removing undesired impurities efficiently and completely.

Reference

1. Itagaki, H.; Koshino, T.; Ito, T.; Sano, T.; Ito, D.; Sugimura, H., Volume Phase Transition of Chemically Cross-linked Curdlan Hydrogels Dependent on pH. *ACS Biomaterials Science & Engineering* **2016,** *2* (5), 752-757.

2. Toledano, S.; Williams, R. J.; Jayawarna, V.; Ulijn, R. V., Enzyme-Triggered Self-Assembly of Peptide Hydrogels via Reversed Hydrolysis. *Journal of the American Chemical Society* **2006,** *128* (4), 1070-1071.

3. Yang, Z.; Ma, M.; Xu, B., Using matrix metalloprotease-9 (MMP-9) to trigger supramolecular hydrogelation. *Soft Matter* **2009,** *5* (13), 2546-2548.

4. Hacker, M. C.; Klouda, L.; Ma, B. B.; Kretlow, J. D.; Mikos, A. G., Synthesis and Characterization of Injectable, Thermally and Chemically Gelable, Amphiphilic Poly(N-isopropylacrylamide)-Based Macromers. *Biomacromolecules* **2008,** *9* (6), 1558-1570.

5. Kesti, M.; Müller, M.; Becher, J.; Schnabelrauch, M.; D'Este, M.; Eglin, D.; Zenobi-Wong, M., A versatile bioink for three-dimensional printing of cellular scaffolds based on thermally and photo-triggered tandem gelation. *Acta Biomaterialia* **2015,** *11*, 162-172.

6. Sun, A. X.; Lin, H.; Fritch, M. R.; Shen, H.; Alexander, P. G.; DeHart, M.; Tuan, R. S., Chondrogenesis of human bone marrow mesenchymal stem cells in 3-dimensional, photocrosslinked hydrogel constructs: Effect of cell seeding density and material stiffness. *Acta Biomaterialia* **2017,** *58*, 302-311.

7. Li, R.; Horgan, C. C.; Long, B.; Rodriguez, A. L.; Mather, L.; Barrow, C. J.; Nisbet, D. R.; Williams, R. J., Tuning the mechanical and morphological properties of self-assembled peptide hydrogels via control over the gelation mechanism through regulation of ionic strength and the rate of pH change. *RSC Advances* **2015,** *5* (1), 301-307.

8. Zhang, W.; Wang, X.; Wang, S.; Zhao, J.; Xu, L.; Zhu, C.; Zeng, D.; Chen, J.; Zhang, Z.; Kaplan, D. L.; Jiang, X., The use of injectable sonication-induced silk hydrogel for VEGF165 and BMP-2 delivery for elevation of the maxillary sinus floor. *Biomaterials* **2011,** *32* (35), 9415-9424.

9. Hu, W.; Wang, Z.; Xiao, Y.; Zhang, S.; Wang, J., Advances in crosslinking strategies of biomedical hydrogels. *Biomaterials Science* **2019,** *7* (3), 843-855.

10. Zhong, S. P.; Zhang, Y. Z.; Lim, C. T., Tissue scaffolds for skin wound healing and dermal reconstruction. *WIREs Nanomedicine and Nanobiotechnology* **2010,** *2* (5), 510-525.

11. Kondiah, P. J.; Choonara, Y. E.; Kondiah, P. P. D.; Marimuthu, T.; Kumar, P.; du Toit, L. C.; Pillay, V., A Review of Injectable Polymeric Hydrogel Systems for Application in Bone Tissue Engineering. *Molecules* **2016,** *21* (11), 1580.

12. Ma, C.; Gerhard, E.; Lu, D.; Yang, J., Citrate chemistry and biology for biomaterials design. *Biomaterials* **2018,** *178*, 383-400.

13. Dixon, T. F.; Perkins, H. R., Citric acid and bone metabolism. *Biochem J* **1952,** *52* (2), 260-265.

14. Fu, X.; Li, Y.; Huang, T.; Yu, Z.; Ma, K.; Yang, M.; Liu, Q.; Pan, H.; Wang, H.; Wang, J.; Guan, M., Runx2/Osterix and Zinc Uptake Synergize to Orchestrate Osteogenic Differentiation and Citrate Containing Bone Apatite Formation. *Adv Sci (Weinh)* **2018,** *5* (4), 1700755-1700755.

15. Binu, S.; S.J, S.; Sudhakaran, P., Metabolite control of angiogenesis: Angiogenic effect of citrate. *Journal of physiology and biochemistry* **2012,** *69*.

16. Tran, R. T.; Yang, J.; Ameer, G. A., Citrate-Based Biomaterials and Their Applications in Regenerative Engineering. *Annu Rev Mater Res* **2015,** *45*, 277-310.

17. Costello, L. C.; Franklin, R. B.; Reynolds, M. A.; Chellaiah, M., The Important Role of Osteoblasts and Citrate Production in Bone Formation: "Osteoblast Citration" as a New Concept for an Old Relationship. *Open Bone J* **2012,** *4*, 10.2174/1876525401204010027.

18. Ma, C.; Tian, X.; Kim, J. P.; Xie, D.; Ao, X.; Shan, D.; Lin, Q.; Hudock, M. R.; Bai, X.; Yang, J., Citrate-based materials fuel human stem cells by metabonegenic regulation. *PNAS* **2018**.

19. Hu, Y. Y.; Liu, X. P.; Ma, X.; Rawal, A.; Prozorov, T.; Akinc, M.; Mallapragada, S. K.; Schmidt-Rohr, K., Biomimetic Self-Assembling Copolymer−Hydroxyapatite Nanocomposites with the Nanocrystal Size Controlled by Citrate. *Chemistry of Materials* **2011,** *23* (9), 2481-2490.

20. Saravanan, S.; Vimalraj, S.; Thanikaivelan, P.; Banudevi, S.; Manivasagam, G., A review on injectable chitosan/beta glycerophosphate hydrogels for bone tissue regeneration. *International Journal of Biological Macromolecules* **2019,** *121*, 38-54.

21. Kucińska-Lipka, J.; Gubanska, I.; Korchynskyi, O.; Malysheva, K.; Kostrzewa, M.; Włodarczyk, D.; Karczewski, J.; Janik, H., The Influence of Calcium Glycerophosphate (GPCa) Modifier on Physicochemical, Mechanical, and Biological Performance of Polyurethanes Applicable as Biomaterials for Bone Tissue Scaffolds Fabrication. *Polymers (Basel)* **2017,** *9* (8), 329.

22. Song, E.-H.; Cho, K.-I.; Kim, H.-E.; Jeong, S.-H., Biomimetic Coating of Hydroxyapatite on Glycerol Phosphate-Conjugated Polyurethane via Mineralization. *ACS Omega* **2017,** *2* (3), 981-987.

23. Morochnik, S.; Zhu, Y.; Duan, C.; Cai, M.; Reid, R. R.; He, T. C.; Koh, J.; Szleifer, I.; Ameer, G. A., A thermoresponsive, citrate-based macromolecule for bone regenerative engineering. *Journal of Biomedical Materials Research Part A* **2018,** *106* (6), 1743-1752.

24. Rosales-Leal, J. I.; Rodríguez-Valverde, M. A.; Mazzaglia, G.; Ramón-Torregrosa, P. J.; Díaz-Rodríguez, L.; García-Martínez, O.; Vallecillo-Capilla, M.; Ruiz, C.; Cabrerizo-Vílchez, M. A., Effect of roughness, wettability and morphology of engineered titanium surfaces on osteoblast-like cell adhesion. *Colloids and Surfaces A: Physicochemical and Engineering Aspects* **2010,** *365* (1), 222-229.

25. Labriola, N. R.; Azagury, A.; Gutierrez, R.; Mathiowitz, E.; Darling, E. M., Concise Review: Fabrication, Customization, and Application of Cell Mimicking Microparticles in Stem Cell Science. *Stem cells translational medicine* **2018,** *7* (2), 232-240.

26. Hatano, K.; Inoue, H.; Kojo, T.; Matsunaga, T.; Tsujisawa, T.; Uchiyama, C.; Uchida, Y., Effect of surface roughness on proliferation and alkaline phosphatase expression of rat calvarial cells cultured on polystyrene. *Bone* **1999,** *25* (4), 439-45.

27. Martin, J. Y.; Schwartz, Z.; Hummert, T. W.; Schraub, D. M.; Simpson, J.; Lankford, J., Jr.; Dean, D. D.; Cochran, D. L.; Boyan, B. D., Effect of titanium surface roughness on proliferation, differentiation, and protein synthesis of human osteoblast-like cells (MG63). *Journal of biomedical materials research* **1995,** *29* (3), 389-401.

28. Shum, L. C.; White, N. S.; Mills, B. N.; Bentley, K. L. d. M.; Eliseev, R. A., Energy Metabolism in Mesenchymal Stem Cells During Osteogenic Differentiation. *Stem Cells Dev* **2016,** *25* (2), 114-122.

29. Karamanlioglu, M.; Preziosi, R.; Robson, G. D., Abiotic and biotic environmental degradation of the bioplastic polymer poly(lactic acid): A review. *Polymer Degradation and Stability* **2017,** *137*, 122-130.

30. La Mantia, F. P.; Morreale, M.; Botta, L.; Mistretta, M. C.; Ceraulo, M.; Scaffaro, R., Degradation of polymer blends: A brief review. *Polymer Degradation and Stability* **2017,** *145*, 79-92.

31. Ali, S. A. M.; Zhong, S. P.; Doherty, P. J.; Williams, D. F., Mechanisms of polymer degradation in implantable devices: I. Poly(caprolactone). *Biomaterials* **1993,** *14* (9), 648-656.

32. Fetters, L.; Lohse, D.; Richter, D.; Witten, T.; Zirkel, A., Connection between polymer molecular weight, density, chain dimensions, and melt viscoelastic properties. *Macromolecules* **1994,** *27* (17), 4639-4647.

33. Göpferich, A., Mechanisms of polymer degradation and erosion. *Biomaterials* **1996,** *17* (2), 103-114.

34. Laycock, B.; Nikolić, M.; Colwell, J. M.; Gauthier, E.; Halley, P.; Bottle, S.; George, G., Lifetime prediction of biodegradable polymers. *Progress in Polymer Science* **2017,** *71*, 144-189.

35. Langer, R., New methods of drug delivery. *Science* **1990,** *249* (4976), 1527.

36. Farrar, D., Modelling of the degradation process for bioresorbable polymers. In *Degradation rate of bioresorbable materials*, Elsevier: 2008; pp 183-206.

37. Bruggeman, J. P.; Bettinger, C. J.; Nijst, C. L. E.; Kohane, D. S.; Langer, R., Biodegradable Xylitol-Based Polymers. *Advanced Materials* **2008,** *20* (10), 1922-1927.

38. He, Y.; Li, Q.; Ma, C.; Xie, D.; Li, L.; Zhao, Y.; Shan, D.; Chomos, S. K.; Dong, C.; Tierney, J. W.; Sun, L.; Lu, D.; Gui, L.; Yang, J., Development of osteopromotive poly (octamethylene citrate glycerophosphate) for enhanced bone regeneration. *Acta Biomater* **2019,** *93*, 180-191.

39. Tejedor-Tejedor, M. I.; Anderson, M. A., Protonation of Phosphate on the Surface of Goethite As Studied by CIR-FTIR and Electrophoretic Mobility. *Langmuir* **1990,** *6*, 602-612.

40. Holzapfel, G. A., Biomechanics of soft tissue. *The handbook of materials behavior models* **2001,** *3*, 1049-1063.

41. Guo, J.; Wang, W.; Hu, J.; Xie, D.; Gerhard, E.; Nisic, M.; Shan, D.; Qian, G.; Zheng, S.; Yang, J., Synthesis and characterization of anti-bacterial and anti-fungal citrate-based mussel-inspired bioadhesives. *Biomaterials* **2016,** *85*, 204-17.

42. Sung, H. J.; Meredith, C.; Johnson, C.; Galis, Z. S., The effect of scaffold degradation rate on three-dimensional cell growth and angiogenesis. *Biomaterials* **2004,** *25* (26), 5735-5742.

43. Laurencin, C.; Khan, Y.; El-Amin, S. F., Bone graft substitutes. *Expert review of medical devices* **2006,** *3* (1), 49-57.

44. Hu, J.; Peng, K.; Guo, J.; Shan, D.; Kim, G. B.; Li, Q.; Gerhard, E.; Zhu, L.; Tu, W.; Lv, W.; Hickner, M. A.; Yang, J., Click Cross-Linking-Improved Waterborne Polymers for Environment-Friendly Coatings and Adhesives. *ACS Appl. Mater. Interfaces* **2016,** *8*, 17499-17410.

45. Keles, H.; Naylor, A.; Clegg, F.; Sammon, C., Investigation of factors influencing the hydrolytic degradation of single PLGA microparticles. *Polymer Degradation and Stability* **2015,** *119*, 228-241.

46. Loo, J. S. C.; Ooi, C. P.; Boey, F. Y. C., Degradation of poly(lactide-co-glycolide) (PLGA) and poly(l-lactide) (PLLA) by electron beam radiation. *Biomaterials* **2005,** *26* (12), 1359-1367.

47. McKay Fletcher, D. M.; Shaw, R.; Sánchez-Rodríguez, A. R.; Daly, K. R.; van Veelen, A.; Jones, D. L.; Roose, T., Quantifying citrate-enhanced phosphate root uptake using microdialysis. *Plant and Soil* **2019**.

48. Campana, V.; Milano, G.; Pagano, E.; Barba, M.; Cicione, C.; Salonna, G.; Lattanzi, W.; Logroscino, G., Bone substitutes in orthopaedic surgery: from basic science to clinical practice. *Journal of Materials Science: Materials in Medicine* **2014,** *25* (10), 2445-2461.

49. Song, J.; Malathong, V.; Bertozzi, C. R., Mineralization of Synthetic Polymer Scaffolds: A Bottom-Up Approach for the Development of Artificial Bone. *JACS* **2005,** *127* (10), 3366-3378.

50. Bhumiratana, S.; Grayson, W. L.; Castaneda, A.; Rockwood, D. N.; Gil, E. S.; Kaplan, D. L.; Vunjak-Novakovic, G., Nucleation and growth of mineralized bone matrix on silk-hydroxyapatite composite scaffolds. *Biomaterials* **2011,** *32* (11), 2820.

51. Chesnutt, B. M.; Viano, A. M.; Yuan, Y.; Yang, Y.; Guda, T.; Appleford, M. R.; Ong, J. L.; Haggard, W. O.; Bumgardner, J. D., Design and characterization of a novel chitosan/nanocrystalline calcium phosphate composite scaffold for bone regeneration. *J Biomed Mater Res A* **2009,** *88* (2), 491-502.

52. Liang, S. L.; Cook, W. D.; Thouas, G. A.; Chen, Q. Z., The mechanical characteristics and in vitro biocompatibility of poly(glycerol sebacate)-bioglass elastomeric composites. *Biomaterials* **2010,** *31* (33), 8516-8529.

53. Liu, H.; Webster, T. J., Mechanical properties of dispersed ceramic nanoparticles in polymer composites for orthopedic applications. *International journal of nanomedicine* **2010,** *5*, 299-313.

54. Hartles, R. L., Citrate in mineralized tissues. *Adv Oral Biol* **1964,** *1*, 225-253.

55. Chung, E. J.; Kodali, P.; Laskin, W.; Koh, J. L.; Ameer, G. A., Long-term in vivo response to citric acid-based nanocomposites for orthopaedic tissue engineering. *Journal of materials science. Materials in medicine* **2011,** *22* (9), 2131-2138.

56. Guo, Y.; Tran, R. T.; Xie, D.; Wang, Y.; Nguyen, D. Y.; Gerhard, E.; Guo, J.; Tang, J.; Zhang, Z.; Bai, X.; Yang, J., Citrate-based biphasic scaffolds for the repair of large segmental bone defects. *J Biomed Mater Res A* **2015,** *103* (2), 772-781.

57. Sun, D.; Chen, Y.; Tran, R. T.; Xu, S.; Xie, D.; Jia, C.; Wang, Y.; Guo, Y.; Zhang, Z.; Guo, J.; Yang, J.; Jin, D.; Bai, X., Citric acid-based hydroxyapatite composite scaffolds enhance calvarial regeneration. *Sci Rep* **2014,** *4*, 6912.

58. Tran, R. T.; Wang, L.; Zhang, C.; Huang, M.; Tang, W.; Zhang, C.; Zhang, Z.; Jin, D.; Banik, B.; Brown, J. L.; Xie, Z.; Bai, X.; Yang, J., Synthesis and characterization of biomimetic citrate-based biodegradable composites. *J Biomed Mater Res A* **2014,** *102* (8), 2521-2532.

59. Xie, D.; Guo, J.; Mehdizadeh, M.; Tran, R. T.; Chen, R.; Sun, D.; Qian, G.; Jin, D.; Bai, X.; Yang, J., Development of Injectable Citrate-Based Bioadhesive Bone Implants. *Journal of materials chemistry. B, Materials for biology and medicine* **2015,** *3*, 387-398.

60. Tang, J.; Guo, J.; Li, Z.; Yang, C.; Xie, D.; Chen, J.; Li, S.; Li, S.; Kim, G. B.; Bai, X.; Zhang, Z.; Yang, J., Fast degradable citrate-based bone scaffold promotes spinal fusion. *Journal of materials chemistry. B, Materials for biology and medicine* **2015,** *3* (27), 5569-5576.

61. Prasadh, S.; Wong, R. C. W., Unraveling the mechanical strength of biomaterials used as a bone scaffold in oral and maxillofacial defects. *Oral Science International* **2018**.

62. Dey, J.; Xu, H.; Shen, J.; Thevenot, P.; Gondi, S. R.; Nguyen, K. T.; Sumerlin, B. S.; Tang, L.; Yang, J., Development of biodegradable crosslinked urethane-doped polyester elastomers. *Biomaterials* **2008,** *29* (35), 4637-4649.

63. Guo, J.; Xie, Z.; Tran, R. T.; Xie, D.; Jin, D.; Bai, X.; Yang, J., Click chemistry plays a dual role in biodegradable polymer design. *Adv Mater* **2014,** *26* (12), 1906-1911.

64. Holland, T.; Bodde, E.; Cuijpers, V.; Baggett, L.; Tabata, Y.; Mikos, A.; Jansen, J., Degradable hydrogel scaffolds for in vivo delivery of single and dual growth factors in cartilage repair. *Osteoarthritis and Cartilage* **2007,** *15* (2), 187-197.

65. Solchaga, L. A.; Temenoff, J. S.; Gao, J.; Mikos, A. G.; Caplan, A. I.; Goldberg, V. M., Repair of osteochondral defects with hyaluronan-and polyester-based scaffolds. *Osteoarthritis and cartilage* **2005,** *13* (4), 297-309.

66. Liu, Y.; Shu, X. Z.; Prestwich, G. D., Osteochondral Defect Repair with Autologous Bone Marrow–Derived Mesenchymal Stem Cells in an Injectable, In Situ, Cross-Linked Synthetic Extracellular Matrix. *Tissue Enigneering* **2006,** *12* (12), 3405-3417.

67. Goss, S. L.; Lemons, K. A.; Kerstetter, J. E.; Bogner, R. H., Determination of calcium salt solubility with changes in pH and PCO2, simulating varying gastrointestinal environments. *Journal of Pharmacy and Pharmacology* **2007,** *59* (11), 1485-1492.

68. Qiu, H.; Yang, J.; Kodali, P.; Koh, J.; Ameer, G. A., A citric acid-based hydroxyapatite composite for orthopedic implants. *Biomaterials* **2006,** *27* (34), 5845-5854.

69. Coathup, M. J.; Cai, Q.; Campion, C.; Buckland, T.; Blunn, G. W., The effect of particle size on the osteointegration of injectable silicate-substituted calcium phosphate bone substitute materials. *J Biomed Mater Res B Appl Biomater* **2013,** *101* (6), 902-910.

70. Yang, J.; Webb, A. R.; Ameer, G. A., Novel Citric Acid-Based Biodegradable Elastomers for Tissue Engineering. *Advanced Materials* **2004,** *16* (6), 511-516.

71. Jiao, Y.; Gyawali, D.; Stark, J. M.; Akcora, P.; Nair, P.; Tran, R. T.; Yang, J., A rheological study of biodegradable injectable PEGMC/HA composite scaffolds. *Soft Matter* **2012,** *8* (5), 1499-1507.

72. Lee, A. P.; King, W. G., Edible oil deodorizing equipment and methods. *Oil & Soap* **1937,** *14* (10), 263-269.

73. Duyck, C.; Miekeley, N.; Porto da Silveira, C. L.; Aucélio, R. Q.; Campos, R. C.; Grinberg, P.; Brandão, G. P., The determination of trace elements in crude oil and its heavy fractions by atomic spectrometry. *Spectrochimica Acta Part B: Atomic Spectroscopy* **2007,** *62* (9), 939-951.

74. Standards, I. F., STANDARD FOR NAMED VEGETABLE OILS. *CODEX STAN* **1999,** *210-1999*.

75. Kim, H. J.; Kim, D.-G.; Yoon, H.; Choi, Y.-S.; Yoon, J.; Lee, J.-C., Polyphenol/FeIIIComplex Coated Membranes Having Multifunctional Properties Prepared by a One-Step Fast Assembly. *Advanced Materials Interfaces* **2015,** *2* (14), 1500298.

Qiyao Li Vita

1. EXPERIENCE

1.1 Research Assistant

Advisor: Prof. Jian Yang 2015 - 2020 | University Park, PA, USA

1.1.1 Development of Phosphate-presenting Citrate-Based Polymers for Enhanced Bone Regeneration

1.1.2 Immune cell-based drug delivery system with biodegradable fluorescent nanoparticles for brain cancer treatment

1.1.3 Renewable, Degradable Citrate based Resin Columns for Purification of Soybean Oil

1.2 Research Assistant

Advisor: Prof. Matthew Becker, 2013 - 2015 | Akron, OH, USA

1.2.1 Oriented Schwann Cell Growth on Micro/Nano-patterned Polymer Surface with Functional Peptide Gradient

2. EDUCATION

- *Ph.D. in Bioengineering*, Pennsylvania State University 2015 - 2020 | PA, USA
- *M.S. in Polymer Science*, University of Akron 2013 - 2015 | OH, USA
- *B.S. in Polymer Science and Engineering*, Beijing University of Chemical Technology 2010 - 2013 | Beijing, China

3. AWARDS

- PMSE Distinguished Poster Award presented at the 254th ACS National Meeting 08/2017
- First Level of Renmin Scholarship 05/2013
- Sunshine Elastomer Scholarship 03/2013
- Outstanding Leadership Award of BUCT (Top 3%) 12/2012
- Outstanding Student Awards of BUCT (Top 5%) 03/2011

4. LEADERSHIP & OUTREACH ACTIVITIES

- Vice president, Student Chapter of the Society For Biomaterials, Penn State 2017-2020
- Vice president, BMES Graduate Student Association, Penn State 2016-2017
- Exhibitor of Biomedical engineering department on "Career days for girls" 2016
- Representative for Master program, Polymer Science Student Organization, U of Akron 2014-2015
- Teaching assistant on COSI (the Science Museum in Columbus) Science Day at King Elementary School 2013
- Mentored graduate, undergraduate and high school students 2014-2020

5. SELECTED PUBLICATIONS & PRESENTATIONS

1. Y. He#, Q. Li#*, C. Ma, J. Yang*, *et al.*, Development of Osteopromotive Poly (octamethylene citrate glycerophosphate) (POC-GP) for Enhanced Bone Regeneration, Acta Biomaterialia, 2019, 93, 180-191.
2. Q. Li, J. Guo, J. Chen, Y. Zhu, J. Yang, "Synthesis and evaluation of poly(octamethylene citrate β-glycerophosphate) (POC-βGP) for Bone Regeneration", 254th ACS National Meeting, Washington, DC, August 20-24, 2017. (254th ACS National Meeting, PMSE Distinguished Poster Award)
3. W. Zhou, Y. Li, J. Yan, P. Xiong, Q. Li, Y. Cheng*, Y. Zheng, Construction of Self-defensive Antibacterial and Osteogenic AgNPs/Gentamicin Coatings with Chitosan as Nanovalves for Controlled release, Scientific reports, 2018, 8 (1), 13432
4. Y. Ma, G. Policastro, Q. Li, W. J. Landis*, M. L. Becker*, *et al.*, "Concentration Dependent hMSC Differentiation on Orthogonal Concentration Gradients of GRGDS and BMP-2 Peptides", Biomacromolecules, 2016, 17(4), 1486-1495.
5. J. Yang, Q. Li, E. Gerhard, Renewable and Degradable Citrate-based Resins and Filtration Devices for Purification of Liquids, patent pending.